CHALMERS

Investigation of feasibility for an inverter-controlled variable speed drive in a stirling CSP application

A model based approach

Master of Science Thesis

PETER BRUNNSÅKER
MARTIN ÖSTLING

Department of Energy and Environment
Division of Electric Power Engineering
CHALMERS UNIVERSITY OF TECHNOLOGY
Göteborg, Sweden 2012

Investigation of feasibility for an inverter-controlled variable speed drive in a stirling CSP application

A model based approach

PETER BRUNNSÅKER
MARTIN ÖSTLING

Department of Energy and Environment
Division of Electric Power Engineering
CHALMERS UNIVERSITY OF TECHNOLOGY
Göteborg, Sweden 2012

Investigation of feasibility for an inverter-controlled variable speed drive in a stirling CSP application
A model based approach
PETER BRUNNSÅKER
MARTIN ÖSTLING

Department of Energy and Environment
Division of Electric Power Engineering
Chalmers University of Technology
SE–412 96 Göteborg
Sweden
Telephone +46 (0)31–772 1000

Cover:
Stirling CSP system placed in Antalya, Turkey.

Chalmers Bibliotek, Reproservice
Göteborg, Sweden 2012

Investigation of feasibility for an inverter-controlled variable speed drive in a stirling CSP application
A model based approach

PETER BRUNNSÅKER
MARTIN ÖSTLING
Department of Energy and Environment
Division of Electric Power Engineering
Chalmers University of Technology

Abstract

Environmental safe and non-polluting methods for supporting a growing earth population with energy has never been as discussed as during the last years. This thesis is an evaluation of upgrading a concentrated solar power (CSP) plant based on the stirling dish technology with an inverter controlled generator system instead of a system locked to the grid frequency. The purpose is to investigate if the extra energy obtained economically justifies investment in a more efficient but more expensive solution.

This thesis shows that by introducing an inverter controlled drive system, the resulting CSP system is more efficient during the less sunny days as well as during the morning/afternoon hours. The overall annual efficiency for a reference site in Los Angeles, California (USA) increased by 6.7% as well as giving the benefit of not needing to optimize the system for each new installation site. The extra energy produced is shown to justify an investment in an inverter-controlled variable speed drive.

Index Terms: CSP, Concentrating Solar Power, stirling, solar power, green energy.

Acknowledgements

This work has been carried out with the financial support from Consat Engineering AB and the academic support given by the Department of Energy and Environment at Chalmers University of Technology.

Consat Engineering AB is an engineering firm active in the industry. Consat mixes both traditional consulting services and large scale in-house projects where they deliver a complete solution to the client.

The authors would like to express gratitude to the devoted engineers in the project team at Consat Engineering as well as the external owners of the project. Also, not to forget, our supervisor Torbjörn Thiringer at the Division of Electric Power Engineering at the Department of Energy and Environment.

An extra thanks is credited to family and friends who have supported us during the hunt for a Master of Science degree.

Peter Brunnsåker & Martin Östling
Göteborg, Sweden, 2012

Contents

List of Figures

Nomenclature

Superscripts

α	Displacement angle, rad
$\frac{d}{d\theta}$	Derivative with respect to the crankshaft angle, θ
$\frac{d}{dt}$	Derivative with respect to time
γ	Relation between c_p and c_v
ω	Speed, rad/s
θ	Crankshaft angle, radians
d	Diameter in meter
DM	Rate of change of mass with respect to time
F	Friction constant
gA	Mass flow rate, Kg/rad
I	Sun insolation, W/m^2
M	Total mass of gas in one quadrant, Kg
m	Mass, Kg
p	Pressure, Pa
Q	Heat, J
T	Temperature
v	Volume, m^3

Subscripts

amb	Ambient
avg	Average
c	Compression space
ck	Compression space to cooler interface
dc	Dead space, compression space

de	Dead space, expansions space
e	Expansion space
g	Generator
$gear$	Gearbox
h	Heater
he	Heater to expansion space interface
k	Cooler
kr	Cooler to regenerator interface
r	Regenerator
rh	Regenerator to heater interface
s	Stirling engine
sd	Static friction in stirling engine

Abbreviations

AC	Alternating Current
AEO	Annual Energy Outlook
CSP	Concentrated Solar Power
DC	Direct Current
DNI	Direct Normal Irradiance
EEG	German Renewable Energy Act
EIA	Energy Information Administration
EREC	European Renewable Energy Council
KVL	Kirchoff‘s Voltage Law
PCS	Pressure Control System
PCU	Power Converting Unit
PM	Permanent Magnet
PMG	Permanent-Magnet Generator
PMSG	Permanent-Magnet Synchronous Generator
PMSM	Permanent-Magnet Synchronous Machine
PV	Photovoltaic
RES-E	Renewable Energy-Sourced Electricity
SVM	Space Vector Modulation
TCS	Temperature Control System

Chapter 1

Introduction

1.1 Background

It's 2012 and green energy is discussed more then ever. After the earthquake and following tsunami in Japan 2011 and the following destruction of nuclear power plants, countries has started to reconsider whether they should go for nuclear power or not. Germany, for instance, made the decision of shutting down their nuclear power plant park. The aim in Germany is to replace all nuclear power with green energy in form of solar and wind power. To make the green energy reform possible, it need to be efficient and have the possibilities to deliver sufficient power to the grid 24 hours per day and to make this possible a combination of different technologies depending on the local environment and possibilities is needed. Solar power is growing both in efficiency and installations every year. However, as with all technologies it needs to increase in efficiency to make it less costly to install and handle and therefore be able to compete with fossil fuels and nuclear power.

1.2 Project description

The CSP (Concentrating Solar Power) technology is based on concentrating as much sunlight as possible via a parabolic mirror on to a receiver. The receiver is in connection to a stirling engine. Based on temperature differences in the engine, mechanical power output is generated and electricity is produced by connecting a generator to the drive shaft of the stirling engine, see Figure 1.1.

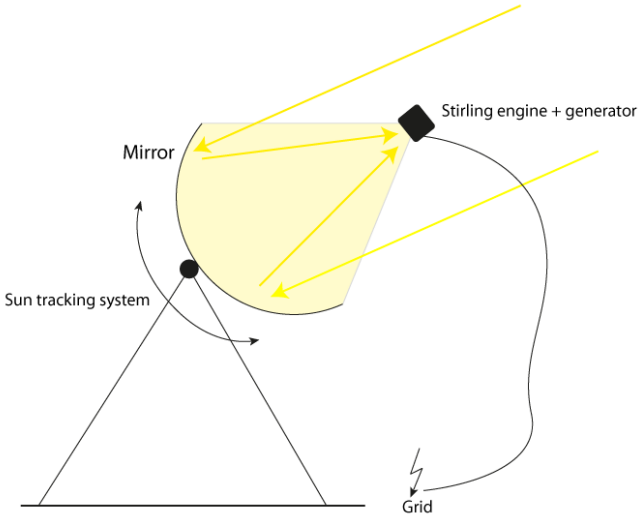

Figure 1.1: Principle for a dish stirling CSP system.

Given for this thesis is a reference plant. The reference plant utilizes a directly driven asynchronous machine as generator. An advantage is that asynchronous machines are cheap as well as easy to connect to the existing power grid, since the machine produces power at the correct power frequency as long as it is connected to a functional power grid. A downside is that the machine operates at an almost constant speed proportional to the grid frequency. The characteristics of the directly driven asynchronous machine affects the stirling engine as well since its mechanically connected. Since the stirling engine do not have an fixed ideal-speed operating point at different inputs there is room for improving the efficiency by being able to speed control this system. Speed controlling can be done using a permanent-magnet (PM) drive, in which a frequency converter is used to change the frequency.

1.2.1 Purpose

This thesis aims to investigate the feasibility of a variable speed drive in a dish stirling system. This is done by comparing a concept plant that utilizes a variable speed drive as generating system with a reference plant that utilizes a directly driven asynchronous machine as generator. The concept- and reference-plant performance is to be compared using mathematical models of that plants implemented in MATLab Simulink. The output over a year as well as the output over a number of chosen reference days is compared. Based on the results in the comparison a short economical evaluation regarding economical profitability for investing in a variable speed drive for a dish stirling application is made.

1.2.2 Limitations

The aim of this thesis is to investigate whether it is economical feasible to implement a variable speed solution, i.e is the extra energy output worth the extra cost for the PM drive including a power conversion system and development of new control algorithms.

- This thesis evaluates the system on a static basis, meaning that the dynamic properties of the components is not considered.
- Evaluation of final result will be based on modelled and simulated systems. No real-life application tests will be performed, however the models will be verified against available measured data from the reference plant.

- This thesis does not treat clusters of stirling dish concentrators. Focus lies on one plant with one mirror, one stirling engine and one generator.

Chapter 2

Theory

2.1 Renewable Energy

Finding new and more efficient ways of gathering energy from renewable energy resources is of great interest when earths natural resources of oil, gas and uranium is running out. Renewable energy resources is typically sunlight, wind, rain, tides and geothermal heat. This thesis focus on the sun as energy resource, therefore only different technologies for harvesting energy from the sun is presented.

The most commercial recognized way to gather energy from the sun is to use photovoltaic (PV) cells, see Figure 2.1(a), to directly convert solar radiation into direct current. Commercial available PV-panels has an efficiency around 10-20% [2]. These types of system are used in both large and small scale applications. For example these panels can be put on rooftops, satellites, boats and other remote systems that need direct power but they are also put in large solar farms.

(a) Photovoltaic solar panels.

(b) Parabolic trough solar farm.

(c) Stirling dish concentrator system.

(d) Solar tower plant.

Figure 2.1: Renewable energy with sun as source.

Concentrated Solar Power (CSP) systems categorises systems where a large area of sunlight is concentrated using lenses or mirrors. There are four main types of CSP systems, namely linear Freshnel reactors, solar power tower, parabolic trough and dish stirling concentrators.

Parabolic trough is a CSP system where parabolic mirrors focus the sunbeams to heat oil which drives a steam turbine to produce electricity, see Figure **??**. The overall efficiency for a parabolic trough system is around 15% [3].

Stirling dish concentrators uses a parabolic mirror to focus the sunlight onto a stirling engine which drives an electric generator, see Figure 2.1(c). The overall efficiency for this type of system is highest of all solar technologies, around 30% [4].

Solar power tower consists of an array of flat mirrors which are moveable, see Figure 2.1(d). The mirrors track the sun and focus the heat onto a tower, called the collector. In the collector a working

fluid is heated to drive a steam turbine. This technology has been proven to work good and has the advantage of being quite simple in design and work. The efficiency is approximately 10-15% [5].

The amount of energy produced from these renewable energy resources is expected to increase by many multiples in coming years. 2010 Europe alone installed 13.2 GW of solar power and for the first time more solar- than wind-power was installed. To match the upcoming expansion in this market, manufactures constantly develop their products to be as efficient as possible. Anticipated annual growth in thermal solar energy in USA is 3.2% until year 2035 [6]. Increase of photovoltaic panels is expected to be even higher than solar thermal power. USA had by the end of 2010 a total of 509 MW (PV) and signed contracts for an additional 7.7 GW [7]. EREC [8] estimates an annual growth of about 35% for solar thermal power in Europe between 2010-2020. Spain currently has 632 MW installed and plans to have 1789 MW installed solar thermal power installed by the end of 2013. Germany introduced the German Renewable Energy Act (EEG) in year 2000. The purpose of this was to promote renewable energy-sourced electricity (RES-E), including wind, hydro and solar power. Between the years 2000 and 2007, Germany increased the green energy generation from 37 TWh to 87 TWh, where PV panels stood for about 4.3% of the generated power [9]. in 2012, Germany had a peak effect 22GW per hour from PV-panels only [10].

2.2 Insolation

The sun provide our planet with sunlight that support almost all life on Earth with photosynthesis. The radiant light and heat from the sun has been harnessed by the human race for millenniums. The technologies used has constantly evolved over the years. One way of quantifying the amount of solar energy is to use the concept insolation. Insolation is a measurement of how much solar radiation energy that is received on a given surface area at a given time. The output from a CSP plant is highly dependent on the insolation since this is the input to the system. To maximize the output it is therefore important to have as high insolation, power input, as possible over as long time as possible. Based on these prerequisites there are certain geographical areas that is more suitable to place a CSP system.

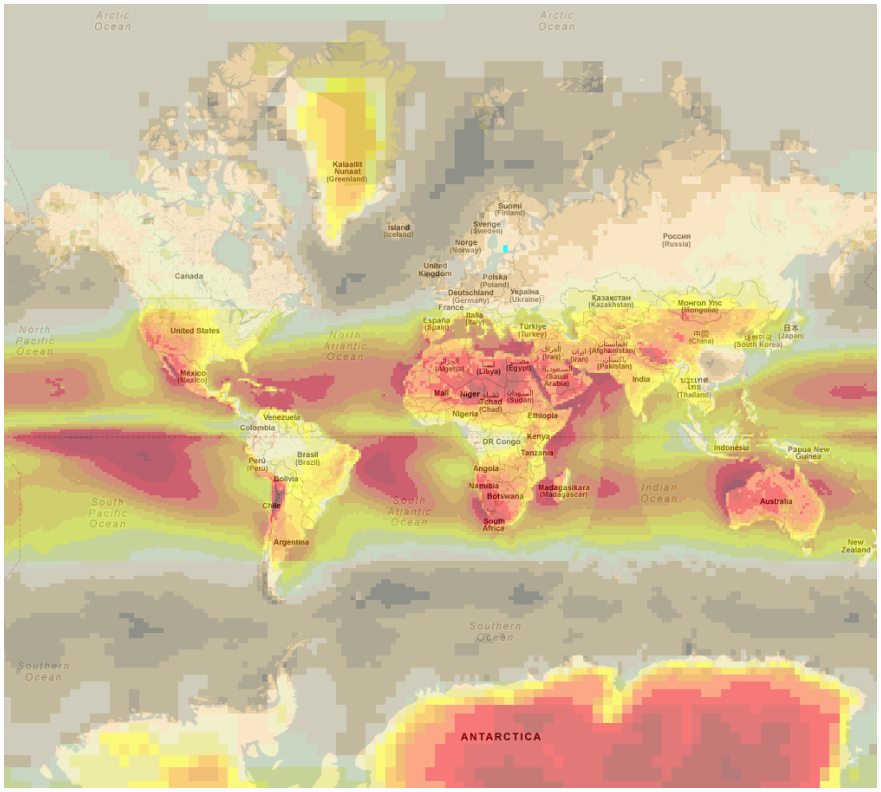

Figure 2.2: Average annual DNI measured by NASA [1].

In Figure 2.2, measurements made by NASA [1] showing average annual Direct Normal Irradiation (DNI) is presented. This gives a hint to where it is suitable to place a CSP system. To make the decision of installing a plant in reality of course involves a lot of other factors to take in to consideration, such as availability of power grid, terrain, surrounding temperature, permits and infrastructure.

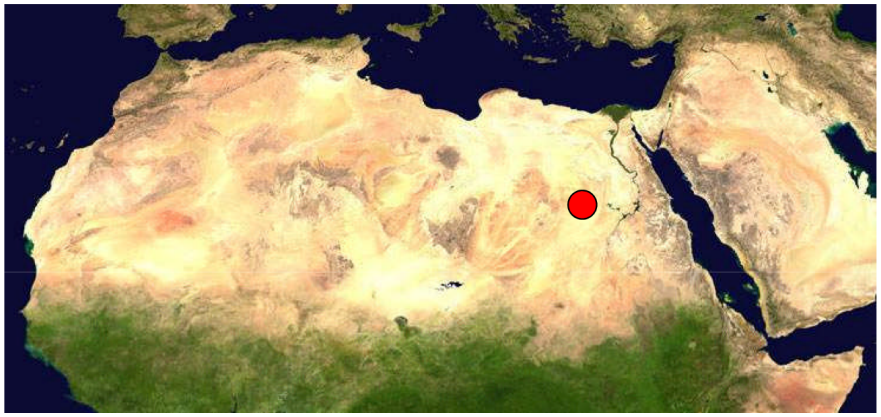

Figure 2.3: CSP potential versus electricity demand.

In Figure 2.3 the red dot represents one percentage of Sahara desert. The insolation received on that area would be enough to supply the worlds entire energy demand using CSP technology. In practice this would be about four times larger because the plants can't be placed to close to each other due to that they would shadow each other. But this gives a good picture about the potential for CSP system.

Just looking at pure energy from the sun and not considering the other factors mentioned above this seems like a good idea, but in practice placing a CSP system in the middle of the Sahara desert is not yet viably.

2.3 The CSP stirling dish system

The purpose of a stirling dish system is to produce electricity. To understand how this is achieved the stirling dish system is divided into smaller subsystems in this chapter.

2.3.1 Concentrator

The solar energy is concentrated onto the Power Concentrating Unit (PCU) by mirrors placed in a parabolic-dish-shaped frame. The mirrors are angled to focus all incoming solar energy onto the absorber in the receiver. The size of the concentrator depends on how much power input the PCU can handle and also on the efficiency of the concentrator itself. For a 25 kW system a dish with approximately 10 meters diameter is needed [11]. The reflective surface is often of aluminium or silver protected by either glass or plastic. Tests has also been made with thin polymer films that are coated in aluminium or silver on the front or back. The ideal shape of the concentrator reflective surface would be to have the whole dish made in a single piece parabolic-dish-shaped reflector. However that would require complex manufacturing, impractical handling and require the whole reflective surface to be replaced/repaired if defections are discovered. In practice therefore the concentrator consists of a number of segments that together form the dish-parabolic-shape. Most commonly these surfaces are round or square but there are also plants with surfaces of more complex geometries. The efficiency of the concentrator without considering tracking of the sun and meteorological effects is determined by the reflectivity of the surfaces and the shape of the dish. Reflectivity losses increases with time as debris is gathered onto the mirrors.

2.3.2 Tracker

To maximize the solar input to the engine, a sun-tracking system guarantees that the concentrator always stays directed towards the sun. Because the concentrator concentrate solar energy in two dimensions, the tracking system must also track the sun's path along two axes.

2.3.3 Receiver

The concentrator focus the incoming solar energy onto a receiver. The receivers task is to absorb as much of the solar energy reflected by the concentrator as possible and transfer this energy as heat to heat the working gas in the stirling engine. To minimize heat losses the receiver is often isolated. Inside the receiver, exposed to the environment is an absorber placed, the task of the absorber is to capture the sun rays and transfer the heat to the working gas. The absorber consists of a mesh of tubes connected to the top of the cylinders of the stirling engine in the power concentrating unit. Inside these tubes the working gas flows. The temperature of the absorber is critical for the efficiency of the stirling engine. The temperature is to be maintained as high as possible while not exceeding the thermal limits of the material for the receiver and absorber. And since the controller controls the maximum temperature in the absorber it is important that the temperature is evenly distributed over the exposed absorber surface.

2.3.4 Power Concentrating Unit (PCU)

In the PCU, conversion from solar energy to mechanical energy is done using a stirling engine, see Section 2.4. The drive shaft of the stirling engine is then connected to an electrical generator which converts the energy to electricity. A system for providing working gas is placed in the PCU. This typically consists of a high pressure tank which supply working gas when the pressure inside the engine is to be raised and a low pressure dump tank which is used for dumping gas when the pressure is to be lowered. Because working gas is leaked in stirling engines through seals and joints the working gas system can not be seen as a closed system.

2.4 Stirling Engine

A stirling engine is operating by cyclic compression and expansion of a working gas. The working gas could be either some type of gas or some type of liquid, most commonly air, hydrogen or helium. Expansion and compression is achieved by heating and cooling the working gas in separate chambers and moving the gas between them through different compartments. The stirling engine is known for having quiet operation and high efficiency. It operates on any type of heat source, have long life and is non-polluting [12].

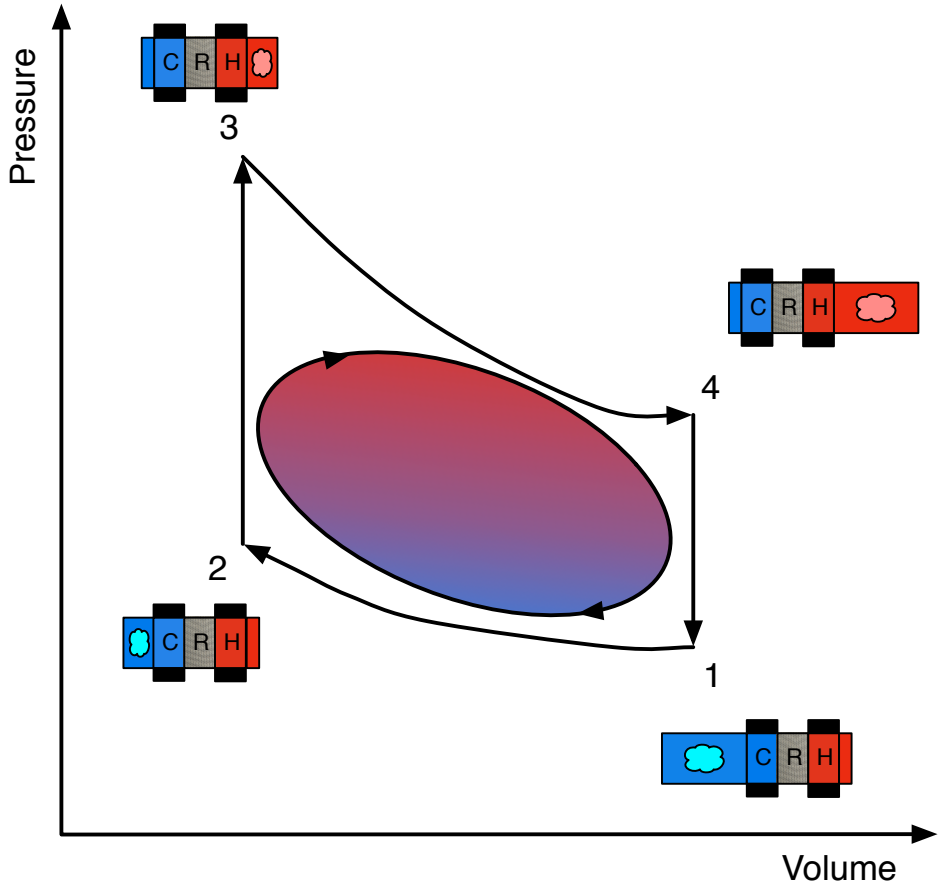

Figure 2.4: Overview of the stirling cycle.

Looking at the stirling circle in a pressure-volume diagram in Figure 2.4 the cycle consists of two constant-volume processes and two isothermal processes. Transition 1-2 is an isothermal compression of the working gas since the process uses the flywheel momentum. Transition 2-3 is a constant volume process where the working gas is transferred to the hot space. Transition 3-4 is an isothermal expansion of the working gas achieved by heating the working gas. Transition 4-1 is a constant volume process where the working gas is moved to the cold space. The net work generated during each cycle is equal to the area of the enclosed curve.

An ideal stirling cycle has an efficiency equivalent to the Carnot cycle [13], which is given by $\mu = 1 - T_3/T_1$ where T_1 refers to point 1 in Figure 2.4. The real cycle differs from the ideal one and can be seen as a oval in Figure 2.4.

As discussed above a stirling engine typically has five important compartments per quadrant in the motor. Compression space, cooler, regenerator, heater and expansion space. The cooler removes heat from the working gas, often by water cooling or forced air convection. The regenerator is a compact cylinder of wire mesh with the intention to recapture some of the energy when the hot and cold working fluid is moved between the hot and cold side. The regenerator greatly improves the efficiency of the stirling engine and is the main contribution of Robert Stirling who has named the stirling engine. In the heater the working gas is heated. Since a stirling engine operates in a closed cycle the heat must be transferred from the external heat source to the working gas through some solid.

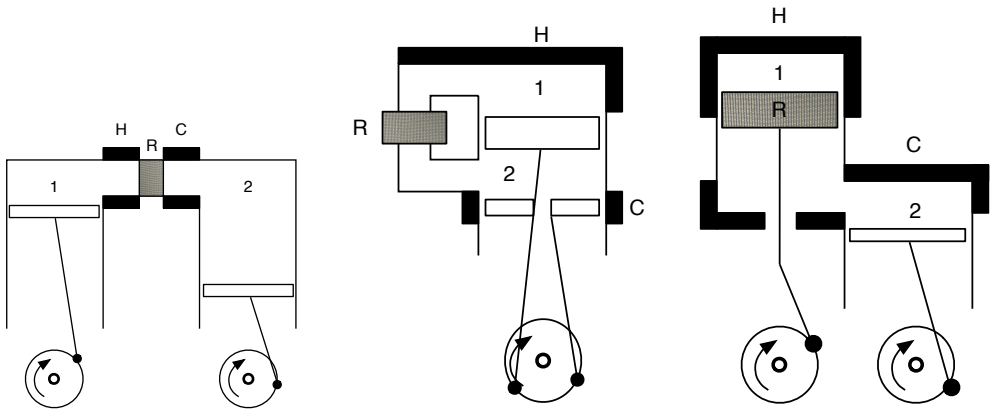

(a) Alpha type stirling engine (b) Beta type stirling engine (c) Gamma type stirling engine

Figure 2.5: Stirling engine types

There exist several configurations of stirling engines, these can usually be divided into three types of stirling engines, seen in Figure 2.5.

The Alpha type stirling engine, see Figure 2.5(a), consist of pistons working in independent cylinders, the gas is compressed in the cold space, moved to the hot space, expansion occurs and the gas is then moved back to the compression space again.

The Beta and Gamma type stirling engine, see Figure 2.5(b) and Figure 2.5(c), uses one piston and one displacer. The displacer separates the hot and cold sides. Working gas must be allowed to pass between the compartments beside the displacer and the cylinder wall. In a Beta type engine the displacer and piston are placed in line. In a Gamma type engine the displacer is placed with an offset to the piston to allow a simpler mechanical arrangement.

2.5 Engine compartment theory

Before introducing any models of the system, some basic equations of thermodynamics as well as basic assumption is given. The double acting alpha stirling engine can be generalized in five separate compartments: Compression space, Cooler, Regenerator, Heater and Expansion space. Each one of them can be generalized accordingly to Figure 2.6.

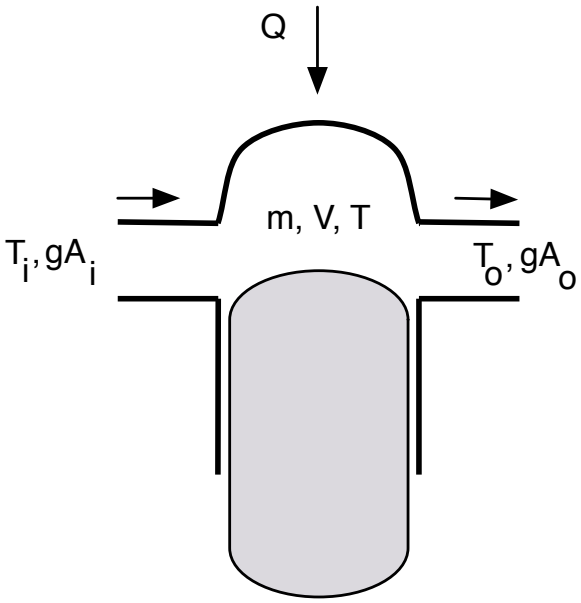

Figure 2.6: A generalized engine compartment.

$$\frac{d}{d\theta}Q + c_p(T_i g A_i - T_o g A_o) = \frac{d}{d\theta}W + c_v\frac{d}{d\theta}(mT) \tag{2.1}$$

- Q Heat (J)
- c_p Specific heat capacity at constant pressure ($J/(Kg \cdot K)$)
- T_i Temperature of incoming gas (K)
- T_o Temperature of outgoing gas (K)
- gA_i Mass flow rate of incoming gas (Kg/rad)
- gA_o Mass flow rate of outgoing gas (Kg/rad)
- W Work done by the cell (J)
- c_v Specific heat capacity at constant volume ($J/(Kg \cdot K)$)
- m Mass of gas within the cell (Kg)
- T Temperature of gas within cell (K)

By using the first law of thermodynamics, an energy balance of the compartment can be made, giving the relationship (2.1) and assuming that the gas behaves ideal, the relations between the pressure, volume, mass and temperature can be expressed as

$$pv = mRT \tag{2.2}$$

- p Pressure (Pa)
- v Volume (m^3)
- m Mass (Kg)
- R Gas constant ($J/(Kg \cdot K)$)
- T Temperature (K)

By differentiating (2.2), taking the natural logarithm of each side, the differential form of the ideal gas equation is expressed as

$$\frac{\frac{d}{d\theta}p}{p} + \frac{\frac{d}{d\theta}v}{v} = \frac{\frac{d}{d\theta}m}{m} + \frac{\frac{d}{d\theta}T}{T} \tag{2.3}$$

Equations (2.1)-(2.3) is in its turn used to define the different compartments in Chapter 3.2.

2.6 Power calculations

Efficiency, power output and power losses are used to compare systems and subsystems. Calculation of power depends on how the energy is stored, such as mechanical energy or electrical energy. Calculation of different powers used in this thesis is done as

$$P_{mech} = \tau\omega \tag{2.4}$$
$$P_{elec} = UI \tag{2.5}$$
$$P_{heat} = EC_a \tag{2.6}$$

where U is the voltage and I is the current, E is the irradiance (W/m^2) and C_a is the applied area (mirror area in this case). The system and subsystem efficiencies are then calculated based on input and output power of the examined system as

$$\eta = \frac{P_{out}}{P_{in}} \tag{2.7}$$

2.7 Machines

2.7.1 Asynchronous machine / Induction machine

The induction machine is very common in industry, about one third of all electricity generated over the world is converted back to mechanical energy in induction machines [14]. An asynchronous machine has an AC-supply and unlike a DC-motor which needs current to be fed to the rotor, the torque-currents of the induction machine are induced by electromagnetic action. An induction machine will always be cheaper than a similar DC-motor because of its simple construction. The induction machine rotates relative to the stator. The rotor is dragged by the stators rotating magnetic field. If the machine is to

be speed controlled, the best way of doing this is to control the speed of the field i.e. the frequency of the supply current. A rotating magnetic field is produced by coil windings located in the stator. When current is fed to the coils a magnetic flux is produced. For example a 4-pole induction motor means that the flux leaves the stator from two north poles and returns at two south poles. For a 4-pole motor, one revolution takes two cycles of the supply. If the supply frequency is 50 Hz and a 4-pole motor is used, one revolution takes 0.04 s which gives a speed of the field, called synchronous speed (N_s), of 1500 rev/min. The synchronous speed is calculated according to

$$N_s = \frac{120f}{p} \tag{2.8}$$

where p is the number of poles, and f is the supply frequency. The number of poles must be an even integer since every north-pole has an opposite south-pole. The direction of rotation can easily be controlled for a induction motor. Since the direction of rotation depends on in which order the currents reach their maxima. Hence changing the direction of rotation is only a matter of switching the two lines that connects the windings to the supply.

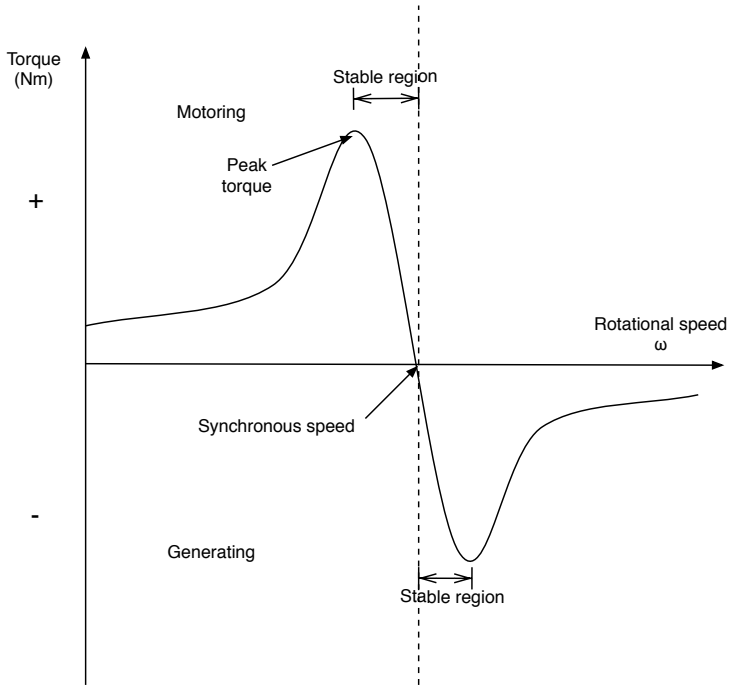

Figure 2.7: Induction machine torque-speed characteristics.

Production of torque in an induction machine is closely related to something called slip. The torque of the rotor depends on its velocity relative to the rotating field. When the rotor is moving below synchronous speed it is dragged by the magnetic field of the stator. If the rotor load increases, but stays below peak torque, the rotor speed will decrease, see Figure 2.7. The slip is known as the relative velocity between the rotor and the field, the larger the slip the larger the currents that are induced in the rotor and thus the larger the produced torque is. The slip is calculated as

$$s = \frac{N_s - N}{N_s} \tag{2.9}$$

An induction machine with no load will have a speed equal to the synchronous speed. If the machine act as a motor the speed will be below synchronous speed. If an induction machine connected to the grid is driven by a mechanical load it will operate above synchronous speed and the machine will act as a generator. The characteristics of the generating region is similar to the region where it acts as a motor, see Figure 2.7.

2.7.2 Permanent magnet synchronous machine

A permanent magnet (PM) machine can be referred to as a synchronous machine or more correctly permanent-magnet synchronous machine (PMSM). For an asynchronous machine, explained in Section 2.7.1, the torque produced is relative to the slip. The speed of an asynchronous motor is always below synchronous speed in practice, and as the load increases the slip increases [14]. In a PM machine the rotor consists of permanent magnet that will create a rotating magnetic field that has the same frequency as the supplying grid frequency. Therefore a synchronous machine, when synchronized, will always run at synchronous speed as long as the torque is below rated peak torque for the machine, both when running as a motor and as a generator. The synchronous speed is calculated according to (2.8).

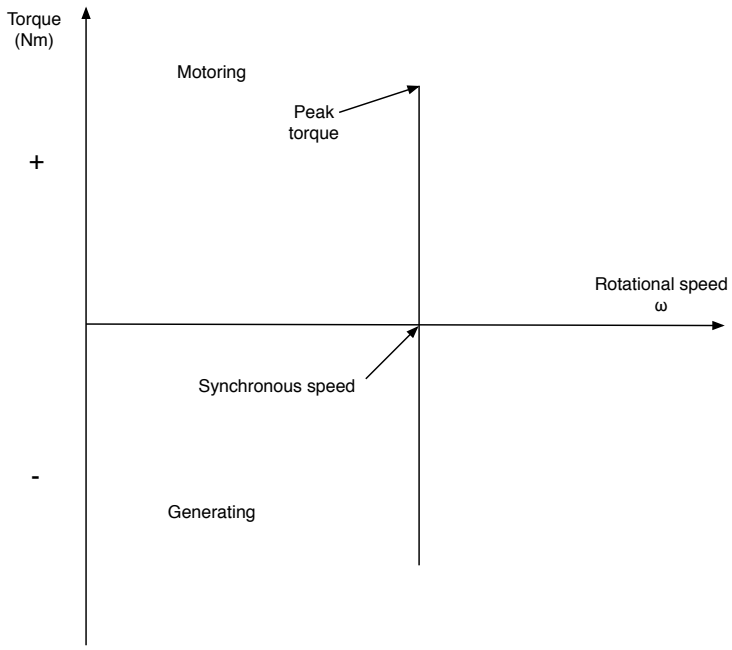

Figure 2.8: PM machine torque-speed characteristics.

The torque speed characteristics for a synchronous machine can be seen in Figure 2.8. Since the speed only depends on the supply frequency, speed controlling a synchronous machine is done through varying the supply frequency. This is done through a converter.

Deriving the electrical equations for a synchronous machine is achieved by applying Kirchoff‘s voltage law (KVL) on each winding. In order to express the voltage drop across a winding, the total magnetic flux produced by the winding need to be known.

2.8 Inverter Controlled Drive

For a system, where a variable-speed power conversion is used, manipulation of the produced signals need to be done since they consist of an AC-voltage which varies over time, as well as a varying frequency. The AC voltage from the PMSG is normally converted into a DC link, which later is fed through a grid connected converter to produce a smooth constant frequency/voltage AC output to the grid [15]. An overview of the conversion system is shown in Figure 2.9.

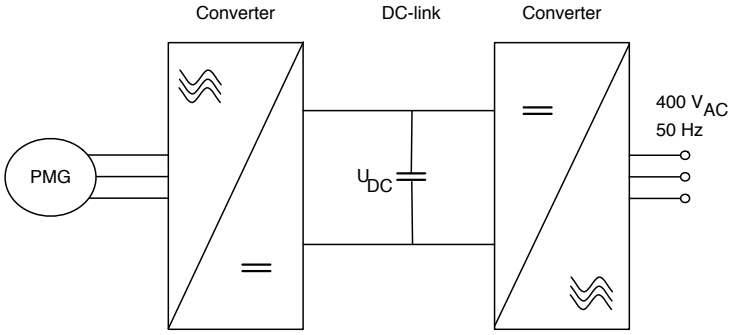

Figure 2.9: Inverter controlled drive system schematics

2.8.1 Back-to-back PWM converter

To convert the power as described above, the signals are first rectified to a DC-voltage via a set of transistors that converts the variable frequency input power to a smooth DC link. The conversion is made with Pulse-Width Modulation (PWM) technique. By firing the transistors in a defined control sequence matching the power frequency a smooth DC voltage is achieved and stored in a capacitor, see Appendix A. In the same way, the smooth DC linkage can be converted into a stable AC output voltage suitable for grid connection. A more detailed schematics of the system is shown in Figure 2.10 [16].

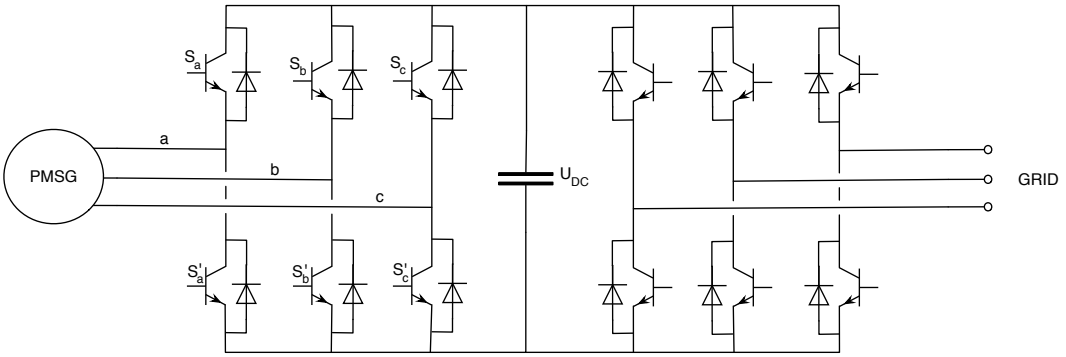

Figure 2.10: Back-to-back PWM conversion schematics

In Figure 2.10 S_a, S_b and S_c represent the switch state. The switch state can just like a bit only have the value 1 which means that the switch is conducting, or 0 which means that the switch is not conducting. To achieve desired output voltages a strategy for controlling the duty cycles of the switches must be derived, this is done in Appendix A. To control the voltages by varying the duty cycles for the switches, equations that relates phase voltages to duty cycles are derived:

$$u_{a0} = \frac{U_{DC}}{3}(2D_a - D_b - D_c) \tag{2.10}$$

$$u_{b0} = \frac{U_{DC}}{3}(-D_a + 2D_b - D_c) \tag{2.11}$$

$$u_{c0} = \frac{U_{DC}}{3}(-D_a - D_b + 2D_c) \tag{2.12}$$

where u_{a0}, u_{b0} and u_{c0} are the respective phase voltages, D_a, D_b and D_c are the respective switch duty cycles and U_{DC} is the DC link voltage. The current in the DC link, i_{DC}, is expressed as:

$$i_{DC} = [D_a \quad D_b \quad D_c] \cdot \begin{bmatrix} i_a \\ i_b \\ i_c \end{bmatrix} \tag{2.13}$$

where i_a, i_b and i_c are the respective phase currents.

2.8.2 Losses in conversion system

By introducing the mentioned PWM converter system, additionally losses is added to the system. These losses consists of power dissipation in the power-supply, gate drives, cooling system and so on. The losses in the power electronic converter can be described as [17]

$$P_{loss} = \frac{P_{conv}}{31}(1 + 10\frac{I_s}{I_{sm}} + 5\frac{I_s^2}{I_{sm}^2} + 10\frac{I_g}{I_{gm}} + 5\frac{I_s^2}{I_{gm}^2}) \tag{2.14}$$

P_{conv}	Dissipation in the converter at rated power (3% of rated power of the converter)
I_g	Grid-side converter current
I_{gm}	Maximum grid-side converter current
I_s	Generator-side converter current
I_{sm}	Maximum generator-side converter current

2.9 Net present value

Net present value (NPV) is a method used for calculating the present value of an investment and then compare this to the investment cost. It is used for decision-support if an investment should be done or not and for comparing different investment-alternatives. The investment is profitable if the net present value is higher then the investment cost. The present value (PV) is calculated as

$$PV = \frac{R}{(1+p)^n} + \sum_{i=1}^{n} \frac{a_i}{(1+p)^i} \tag{2.15}$$

and the net present value is then calculated as

$$NPV = PV - G \tag{2.16}$$

where

NPV	Net present value
R	Residual value
a	Yearly excess
p	Discount rate
n	Investment economical lifetime
i	Year index
G	Investment cost

Chapter 3

Models

For the final analysis to be fair between the two different cases presented in Section 4, a model based on the physical properties of the system is used in favour of measurements. This is mainly due to the fact that the control approach for case two does not exist in real plant, meaning that it can't be measured. However, measurements of the real plant is used to verify that the fundamental model behaves in a correct manner. The mathematical model of the stirling engine as well as the concentrator and receiver is based on the work made by Dustin F. Howard [18].

3.1 Concentrator / Receiver

To collect the solar energy, a parabolic mirror is used to reflect the sunlight in to a small receiver.

$$\frac{d}{dt}Q_I = \pi(\frac{d_{concentrator}}{2})^2\eta_m I = K_c I \tag{3.1}$$

$$\frac{d}{dt}T_h = \frac{1}{\rho c_p V}(\frac{d}{dt}Q_I - \frac{d}{dt}Q_L - \frac{d}{dt}Q_h) \tag{3.2}$$

To represent this system mathematically, a model based on the mirror reflectivity, including losses from misaligned mirrors and possible shadowing from the PCU, is implemented accordingly to (3.1). The heat absorber, which is placed in the receiver is modelled based on heat flows in the system (3.2). Since the heater temperature, T_h should be maintained as high as maximum allowed, to maintain a high efficiency of the engine, a heat flow balance is set-up accordingly to (3.2). From this, it is obvious that the heat flow $\frac{d}{dt}Q_h$ is the main controllable variable to control the heater temperature, since the sun insolation I delivers heat to the system constantly.

The absorber losses, $\frac{d}{dt}Q_L$, is defined as

$$\frac{d}{dt}Q_L = K_L(T_{avg} - T_{amb}) \tag{3.3}$$

where K_L corresponds to a heat loss coefficient based on material and construction of the absorber. $T_{avg} - T_{amb}$ is the difference in the temperature between the average temperature of the absorber and the ambient environment.

3.2 Stirling engine

The stirling engine is modelled as four separated quadrants, each one of them containing a "closed-loop" gas system as in Figure 3.1. The quadrant consists of five separated compartments where the gas

is heated or cooled depending on direction of the flow.

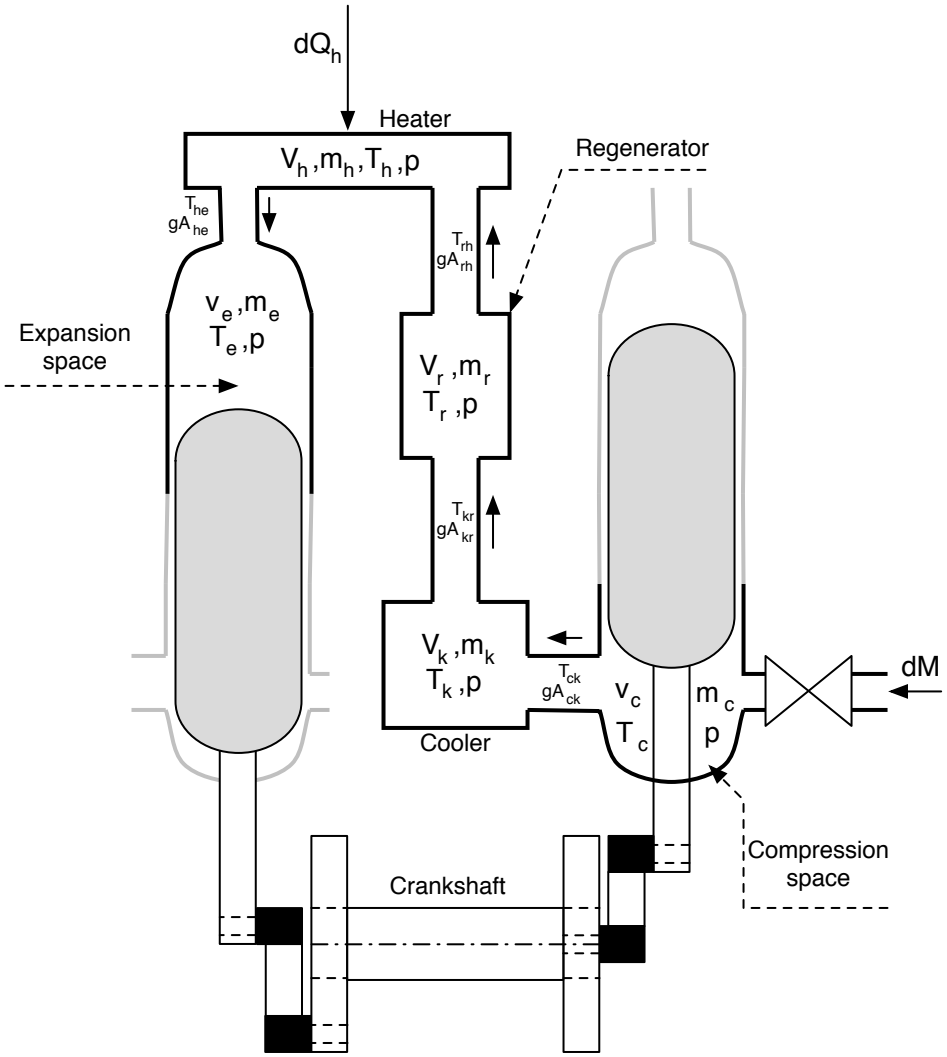

Figure 3.1: The different compartments in one engine quadrant.

3.2.1 Compression space

The volume in the compression space depends on the angle of the crankshaft. Based on (2.2) and knowing the fact that the volume changes with respect to θ and the displacement angle α_c, one easily realise that so will the mass and temperature of the compartment do.

$$v_c = V_{dc} + 0.5V_s[1 + \cos(\theta - \alpha_c)] \tag{3.4}$$

$$\frac{d}{d\theta}v_c = -0.5V_s \sin(\theta - \alpha_c) \tag{3.5}$$

$$\frac{d}{d\theta}m_c = \frac{p\frac{d}{d\theta}v_c + v_c\frac{d}{d\theta}p/\gamma}{RT_{ck}} - \frac{(T_k - T_{ck})\frac{d}{d\theta}M}{T_{ck}} \tag{3.6}$$

$$\frac{d}{d\theta}T_c = T_c(\frac{\frac{d}{d\theta}p}{p} + \frac{\frac{d}{d\theta}v_c}{v_c} - \frac{\frac{d}{d\theta}m_c}{m_c}) \tag{3.7}$$

The physical properties of the compression space is described in (3.4)-(3.7) from where one easily see the connection between for example variations in temperature and the crank shaft angle.

3.2.2 Cooler

The cooler is assumed to be ideal and cool the gas to a constant temperature T_k. This, together with the fixed volume for the chamber, and using (2.1)-(2.3) results in the following for the mass m_k and heat losses Q_k

$$\frac{d}{d\theta}m_k = m_k \frac{\frac{d}{d\theta}p}{p} \tag{3.8}$$

$$\frac{d}{d\theta}Q_k = \frac{V_k \frac{d}{d\theta}p \cdot c_v}{R} - c_p(T_{ck}gA_{ck} - T_{kr}gA_{kr}) \tag{3.9}$$

3.2.3 Regenerator

The temperature in the regenerator depends on which direction the working gas has at the moment. As shown in Figure 3.2, the difference between the temperatures can be described as a function of ΔT. In this case, ΔT is varying with respect to the heater temperature from the absorber accordingly to

$$\Delta T = (1 - \xi) \cdot (T_h - T_k) \tag{3.10}$$

where ξ is the efficiency of the regenerator, thus $\xi = 1$ equals an ideal regenerator and $\xi = 0$ equals no regenerative action [19].

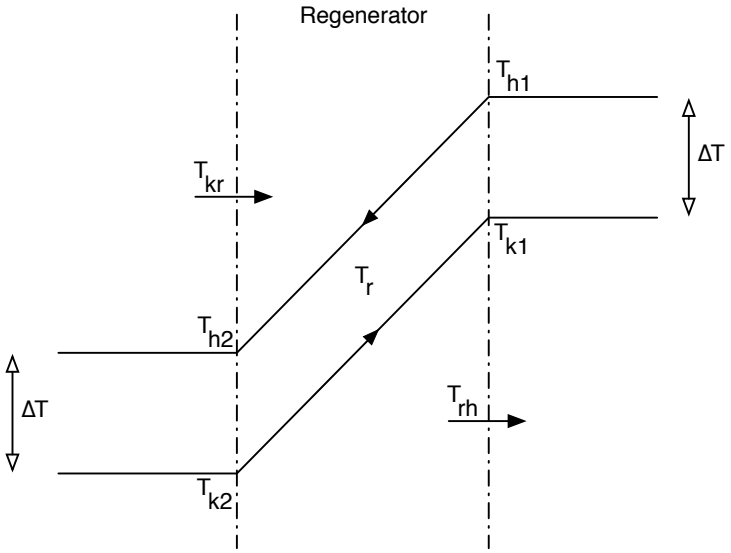

Figure 3.2: Regenerator temperature model

The following physical properties describes the temperature T_r and the change of T_r, m_r, Q_r in the

regenerator

$$T_r = \frac{T_h - T_k}{ln(T_h/T_k)} \tag{3.11}$$

$$\frac{d}{d\theta}T_r = \frac{\frac{d}{d\theta}T_h(ln(T_h/T_k) - 1 + (T_k/T_h))}{ln(T_k/T_h)^2} \tag{3.12}$$

$$\frac{d}{d\theta}m_r = m_r(\frac{\frac{d}{d\theta}p}{p} - \frac{\frac{d}{d\theta}T_r}{T_r}) \tag{3.13}$$

$$\frac{d}{d\theta}Q_r = \frac{V_r\frac{d}{d\theta}p \cdot c_v}{R} - c_p(T_{kr}gA_{kr} - T_{rh}gA_{rh}) \tag{3.14}$$

3.2.4 Heater

The heating temperature T_h is absorbed from the receiver part of the engine. The mass of gas in the heater, m_h, and the gas flow, Q_h, is described as

$$\frac{d}{d\theta}m_h = m_h(\frac{\frac{d}{d\theta}p}{p} - \frac{\frac{d}{d\theta}T_h}{T_h}) \tag{3.15}$$

$$\frac{d}{d\theta}Q_h = \frac{V_h\frac{d}{d\theta}p \cdot c_v}{R} - c_p(T_{rh}gA_{rh} - T_{he}gA_{he}) \tag{3.16}$$

3.2.5 Expansion space

In the same way as the compression space volume, the expansion space volume changes with respect to the crankshaft angle θ and the displacement angle α_e. The properties of the expansion space is described as

$$v_e = V_{de} + 0.5V_s[1 + \cos(\theta - \alpha_e)] \tag{3.17}$$

$$\frac{d}{d\theta}v_e = -0.5V_s\sin(\theta - \alpha_e) \tag{3.18}$$

$$\frac{d}{d\theta}m_e = \frac{p\frac{d}{d\theta}v_e + v_e\frac{d}{d\theta}p/\gamma}{RT_{he}} \tag{3.19}$$

$$\frac{d}{d\theta}T_e = T_e(\frac{\frac{d}{d\theta}p}{p} + \frac{\frac{d}{d\theta}v_e}{v_e} - \frac{\frac{d}{d\theta}m_e}{m_e}) \tag{3.20}$$

3.2.6 Interfaces between compartments

The temperatures and gas mass flow rates between the different compartments mentioned above is varying depending on the crankshaft angle, θ, as well as the effectiveness of the regenerator, as can be seen in Figure 3.3.

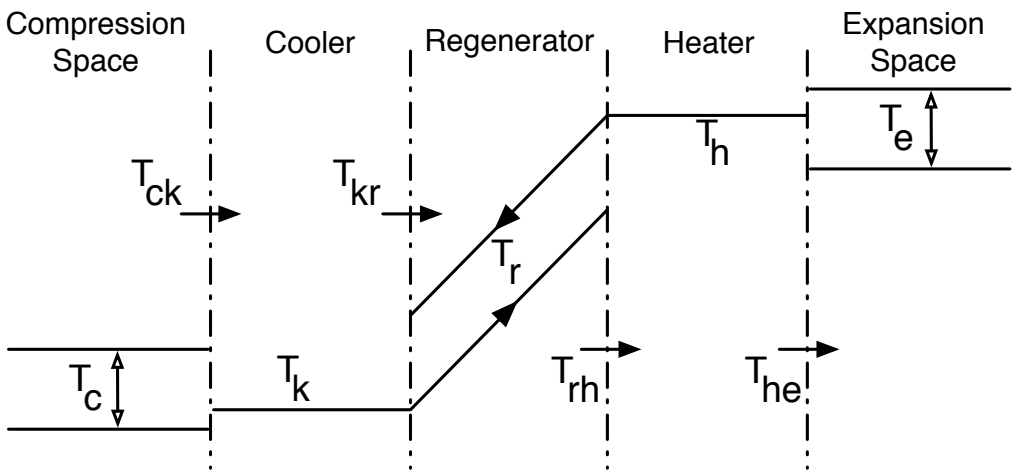

Figure 3.3: Interface temperatures.

The mass flows of the system is described as

$$gA_{ck} = \frac{d}{d\theta}M - \frac{d}{d\theta}m_c \tag{3.21}$$

$$gA_{kr} = gA_{ck} - \frac{d}{d\theta}m_k \tag{3.22}$$

$$gA_{he} = \frac{d}{d\theta}m_e \tag{3.23}$$

$$gA_{rh} = gA_{he} + \frac{d}{d\theta}m_h \tag{3.24}$$

where gA_{xx} corresponds to the gas flow in the interface between the different compartments named accordingly to Figure 3.3. Depending on the sign of the gas flow, the interface temperatures is set accordingly to the following assumptions:

$$\text{if } gA_{ck} > 0, T_{ck} = T_c; \text{ else } T_{ck} = T_k \tag{3.25}$$

$$\text{if } gA_{kr} > 0, T_{kr} = T_k; \text{ else } T_{kr} = T_{h1} \tag{3.26}$$

$$\text{if } gA_{rh} > 0, T_{rh} = T_{k1}; \text{ else } T_{rh} = T_h \tag{3.27}$$

$$\text{if } gA_{he} > 0, T_{he} = T_h; \text{ else } T_{he} = T_e \tag{3.28}$$

3.2.7 Pressure in engine

To control the pressure in the engine, it is evident from (2.2) that the mass of gas is of great importance, which also can be seen in

$$p = \frac{MR}{v_c/T_c + V_k/T_k + V_r/T_r + V_h/T_h + v_e/T_e} \tag{3.29}$$

$$M = m_c + m_k + m_r + m_h + m_e \tag{3.30}$$

$$\frac{d}{d\theta}M = \frac{d}{d\theta}m_c + \frac{d}{d\theta}m_k + \frac{d}{d\theta}m_r + \frac{d}{d\theta}m_h + \frac{d}{d\theta}m_e \tag{3.31}$$

$$\frac{d}{d\theta}p = \frac{\gamma R\frac{d}{d\theta}M(T_k/T_{ck}) - \gamma p(\frac{d}{d\theta}v_c/T_{ck} + \frac{d}{d\theta}v_e(T_{he} - V_r\frac{d}{d\theta}T_r/T_r^2 - V_h\frac{d}{d\theta}T_h/T_h^2))}{v_c/T_{ck} + \gamma(V_k/T_k + Vr/T_r + V_h/T_h) - v_e/T_{he}} \tag{3.32}$$

By controlling the amount of gas in the engine, the pressure is controlled. The total pressure in one of the engine quadrants is calculated by adding (2.2) for each compartment which results in (3.29). The differentiated pressure, (3.32), is derived by inserting the corresponding mass equations for each compartment in combination with the differentiated form of the ideal gas, (2.3). The average pressure in the stirling engine is expressed as the average pressure of the four quadrants:

$$p_{avg} = \frac{p_1 + p_2 + p_3 + p_4}{4} \tag{3.33}$$

3.2.8 Mechanical relations

Each quadrant in the engine delivers torque according to

$$\tau = p(\frac{d}{d\theta}v_c + \frac{d}{d\theta}v_e) \tag{3.34}$$

which explains the relation between pressure in the piston and produced torque, presented by Finkelstein in [20]. Since the modelled engine has four cylinders, equation (3.34) needs to be applied to all for quadrants and summed to get the total output. Adjusting (3.34), results in the following equation for the torque produced by a four piston double-acting configuration

$$\tau_s = p_1(\frac{d}{d\theta}v_{c1} + \frac{d}{d\theta}v_{e1}) + p_2(\frac{d}{d\theta}v_{c2} + \frac{d}{d\theta}v_{e2}) + p_3(\frac{d}{d\theta}v_{c3} + \frac{d}{d\theta}v_{e3}) + p_4(\frac{d}{d\theta}v_{c2} + \frac{d}{d\theta}v_{e4}) \tag{3.35}$$

where the indexes indicates which quadrant that is referred to. Looking at the mechanical connections in Figure 4.1, there is a gear-change between crankshafts and driveshaft.

$$N_{gear} = \frac{k_g}{k_s} \tag{3.36}$$

$$\omega_g = \omega_s\frac{1}{N_{gear}} \tag{3.37}$$

$$\tau_g = \tau_s\eta_{gear}N_{gear} \tag{3.38}$$

The gear ratio is expressed in (3.36) where k represents the number of cogs on the cogwheels. Combining (3.37) and (3.38) express the relationships between torques and speeds.

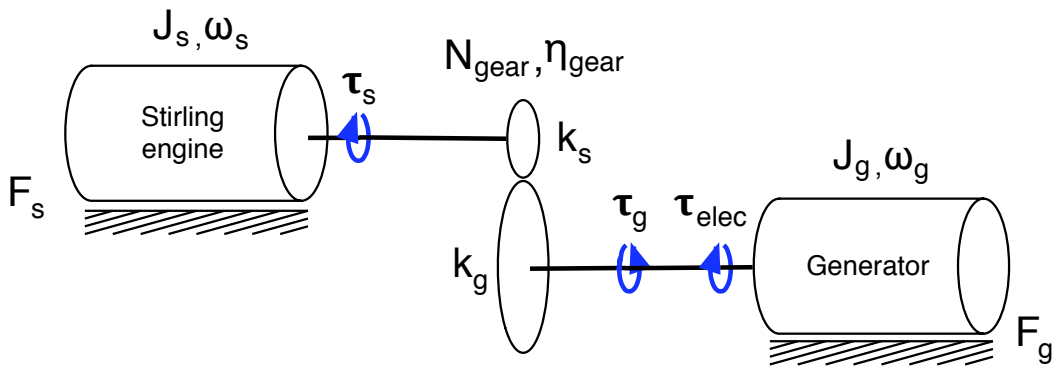

Figure 3.4: Mechanical the mechanical connection from stirling engine to generator.

Using newtons second law of motions to express the rotational equation from Figure 3.4

$$(J_s \frac{1}{N_{gear}} + J_g)\frac{d}{dt}\omega_g = \tau_g - \tau_{elec} - F_g\omega_g - F_s\omega_s - F_{sd} \tag{3.39}$$

3.3 Control of Stirling Engine

According to the carnot cycle (Section 2.4) a heat engine's efficiency is directly proportional to the difference in temperature between the cold and hot side of the engine. Controlling the amount of heat in the absorber is critical for a stirling engine. The temperature of the absorber should be maintained as high as possible, for high efficiency, while not exceeding the thermal limits of the absorber material. The pressure in the engine is another important variable when it comes to efficiency of a stirling engine. It is preferred to have the maximum pressure in the engine as close as possible to the maximum allowed pressure for the engine. The relation between torque and speed can be seen in (3.34). A higher torque means a lower speed if the input stays the same. This means that running on as high pressure as possible translates to running the motor as slow as possible and thus reduce friction losses. In the case when an directly driven asynchronous machine is used as a generator, the rotational speed of the shaft is approximately constant and cannot be controlled. Therefore the only variable available to control the heater temperature is the pressure. In the case when using a variable-speed permanent magnet generator drive system, the controller varies the speed and keeps the pressure at maximum allowed level as long as the system is within an allowed speed interval.

3.3.1 Temperature Control System (TCS)

The most critical variable of the temperature control system (TCS) is the absorber temperature, T_h, since melting components is not desired. If the absorber temperature is not controlled properly while the plant tracks the sun it would only be a matter of seconds before the absorber is melted.

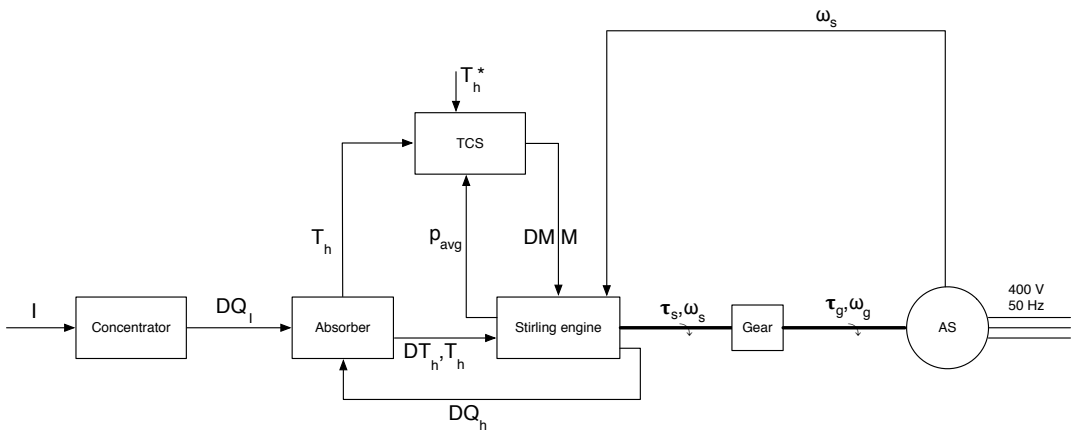

Figure 3.5: Model of overall system with temperature control system.

By using the relationship (2.2) and altering the pressure in the system, the temperature controller keeps the temperature in the system within an allowed interval. The pressure is changed by changing the amount of working gas within the engine compartments, thus the rate of change of the mass of working gas, DM is the main control parameter. A higher amount of working gas in the motor compartments can transfer more heat within the motor, but this also increases the pressure.

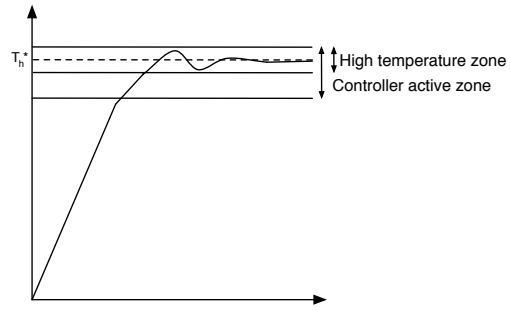

(a) Temperature zones for absorber temperature.

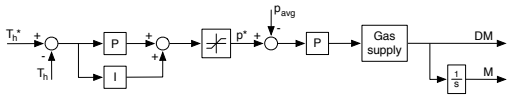

(b) Model of temperature control system.

Figure 3.6: Temperature control.

When the system is to be started the pressure in the system is kept at the low limit and the electric machine used for generating power is instead run as motor. When the system reaches the controlled temperature region, see Figure 3.6(b), the controller is activated and the motor now then dragged by the stirling engine which make it act as a generator instead. The temperature control is done using two nested controllers. An outer gain-scheduled PI-controller that calculates a target pressure based on the difference between target- and current-temperature. The target pressure is then fed into a P-controller that feed a command signal to the pressure and dump tanks.

3.3.2 Pressure Control System (PCS)

When using a variable speed drive, an additional control parameter is introduced to the stirling system since the shaft of the drive is mechanically connected to the stirling engine.

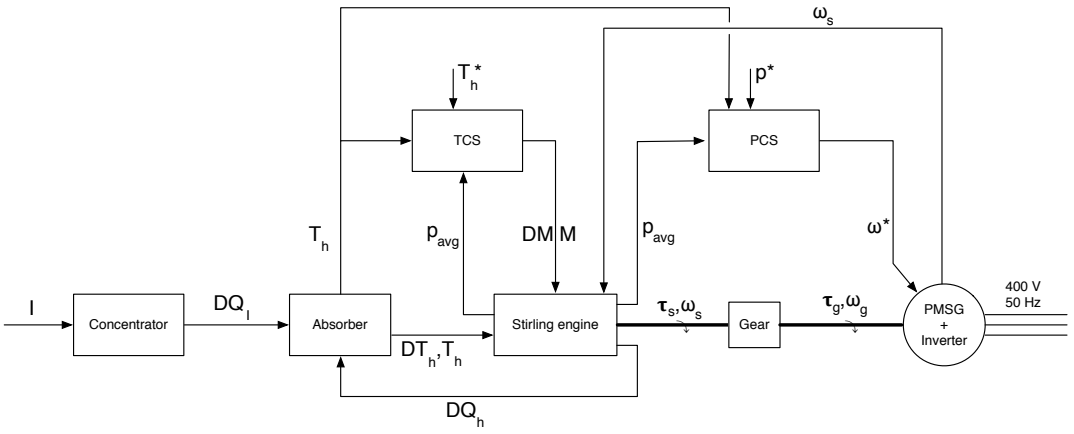

Figure 3.7: Model of overall system with temperature and pressure control system.

As mentioned earlier the efficiency of the stirling engine increases with pressure. The ability of speed controlling the stirling engine will therefore be used for controlling the pressure within the stirling engine to be as high as possible. (3.35) relates torque, speed and pressure.

The TCS control the critical absorber temperature. The TCS is prioritized, in the meaning that the pressure control is not started until the absorber temperature is stabilized within the high temperature zone, see Figure 3.6(a). When the pressure control is inactive the variable speed drive is controlled to act as an directly-driven asynchronous generator.

The variable speed drive has a high- and a low-speed limit. As long as the solar input is sufficient to keep the speed within the allowed speed region the target pressure will be equal to the maximum allowed pressure for the stirling engine. If the input power is not high enough to keep the maximum pressure, while still staying above the low speed limit for the variable speed drive, the pressure will not be controlled. Instead the speed will be kept at the lower limit until the power again is sufficient for the pressure to be kept at the maximum allowed pressure while staying above the low speed limit.

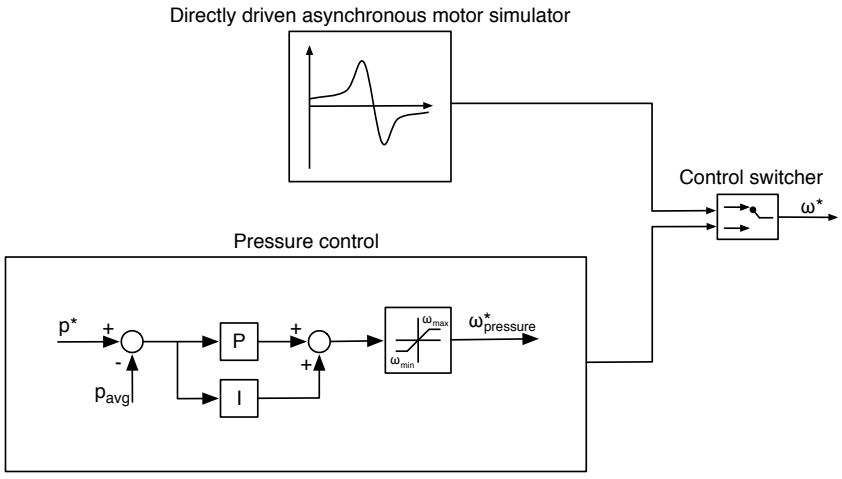

Figure 3.8: Model of pressure control.

Calculation of the desired speed, when pressure control is active, is done in a PI-controller that compares the error between the reference and actual pressure, see Figure 3.8. Output from the PI-

controller is then fed through a saturation block and then passed on to the control system for the variable speed drive. The control system of the variable speed drive is not modelled in detail and is therefore explained in Appendix A.

3.4 Asynchronous generator

The model of the asynchronous generator is based on certification measurements done by Siemens [21]. The data is measured while running the machine as a motor connected to a 400V/50Hz supply. By interpolating the measurements, the efficiency of the directly driven asynchronous generator can be expressed as a function of input power as

$$\eta = 0.00014099 \cdot P_{in}^3 - 0.020243 \cdot P_{in}^2 + 0.82378 \cdot P_{in} + 82.824 \tag{3.40}$$

Comparison between interpolated data and measurements is shown in Figure 3.9.

P [%]	P [W]	I [A]	s [%]	η [%]	$\cos\varphi$ [-]	P_{in} [W]	M [Nm]
26.0	7793	25.7	0.45	88.3	0.495	8830	49.0
51.0	15292	34.0	0.89	92.2	0.705	16586	97.0
76.1	22821	44.2	1.35	93.0	0.801	24542	146.0
100.5	30160	56.0	1.91	92.7	0.838	32527	194.9
101.4	30414	56.1	1.85	92.8	0.844	32770	195.0
125.4	37634	68.2	2.38	92.2	0.864	40810	243.0
150.1	45019	81.8	2.91	91.4	0.869	49270	292.0
169.2	50748	93.1	3.44	90.5	0.870	56080	330.0
188.5	56556	105.2	4.07	89.4	0.868	63240	370.0

Table 3.1: Measured data from certification test of asynchronous generator [21].

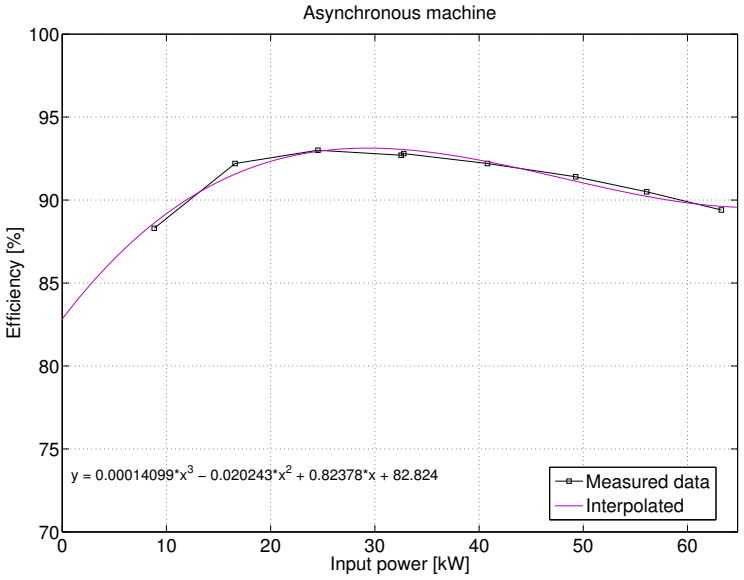

Figure 3.9: Input power vs Efficiency curve for the asynchronous generator.

3.5 PM generator

The variable-speed synchronous drive package consists of one PM generator and one power inverter. Machine data for suitable available products have not been found, however, efficiency mappings for a machine that could be suitable has been found. In [22] a detailed mapping of a 50kW PMSG has been done and in [23] a detailed mapping of the frequency conversion system used in a Toyota Prius hybrid vehicle is made. By choosing the gear ratio wisely, the generator will have an almost constant efficiency of 94% and the conversion system will have an efficiency of 98+%, giving an almost constant drive package efficiency of 92.17%.

Chapter 4

Case set-up

This section presents the case for this thesis. There is a reference plant provided to this project and given the purpose to investigate feasibility of a PM-drive on a dish stirling system, a concept plant is proposed. Both plants consists of a concentrator, a tracker, a receiver and a Power Converting Unit (PCU), see Figure 4.1. The function of these systems will be the same both for the reference and concept plant, see Section 2.3. In the PCU both plants uses a four-cylinder double acting alpha type stirling engine with two cylinders connected to each crankshaft of the stirling engine. The two crankshafts are connected by a cogwheel that also acts as a gear which in its turn is connected to a generator via a drive shaft. The main difference between the two plants is how the generator is operated.

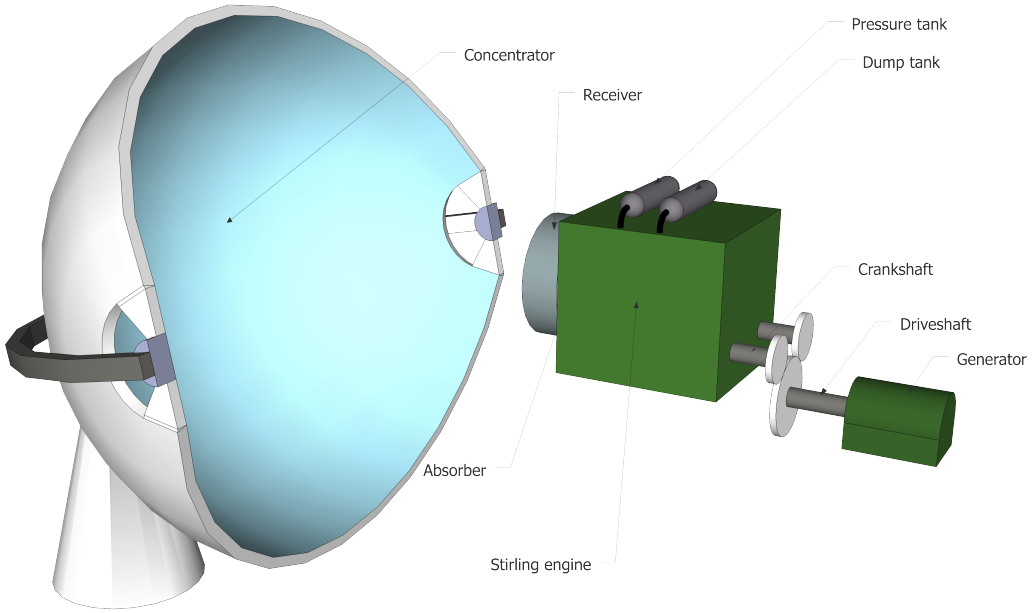

Figure 4.1: Overview of plant.

The overall purpose of a dish stirling system is to convert as much of the sun's heat as possible into electricity. How the energy from the sun varies over a day influences both efficiency and output of the system. Input used for comparing reference plant and concept plant is described in Section 4.1.

4.1 Insolation

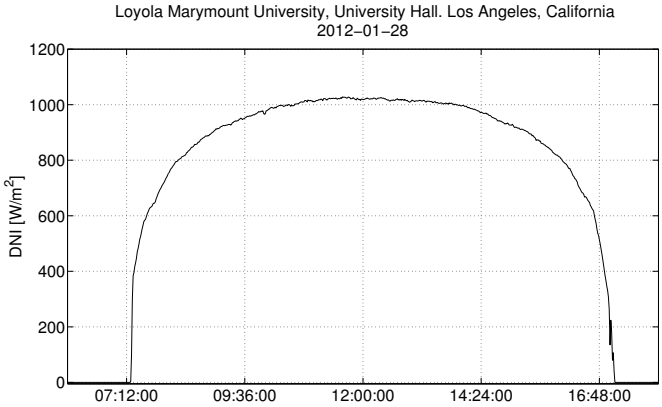

Figure 4.2: Direct Normal Irradiance (DNI) for Los Angeles, California 2012-01-28

Figure 4.2 shows Direct Normal Irradiance (DNI) for Los Angeles, California in the US made by Loyola Marymount University at 2012-01-28 [24]. This measurement shows the characteristics of a good DNI curve for a location where a CSP stirling plant can be placed and will be be used as reference to compare the two plants over a day. However, some days are more cloudy which affects the output from the stirling CSP plant in a negative manner. In Figure 4.3 a more cloudy days characteristics is shown.

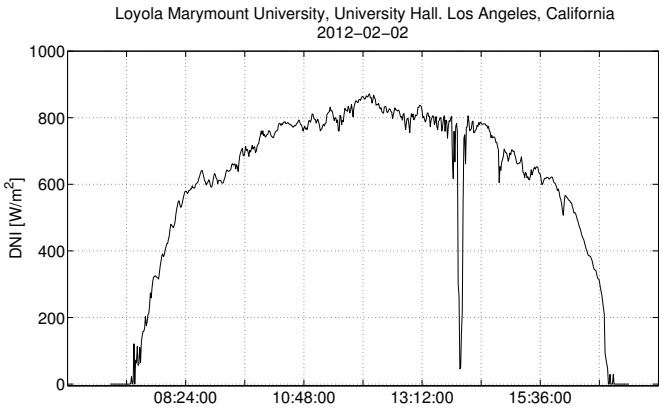

Figure 4.3: Direct Normal Irradiance (DNI) for Los Angeles, California 2012-02-02

If the opposite occurs, meaning that the solar input is a bit higher, the typical DNI data could look as shown in Figure 4.4. This data is not taken from the reference site and it is used only for analysis purpose to show how a non-optimized system could behave.

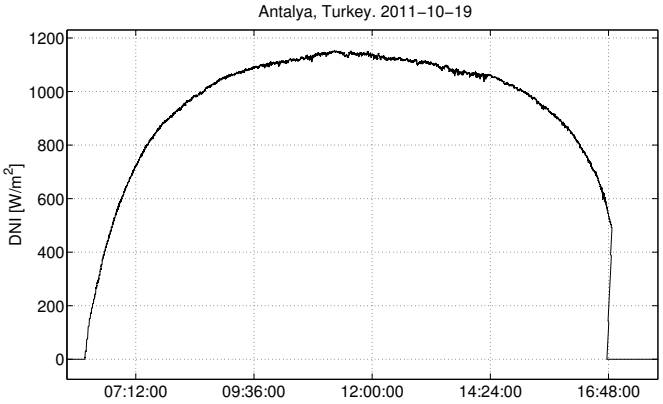

Figure 4.4: Direct Normal Irradiance (DNI) for Antalya, Turkey 2011-10-19

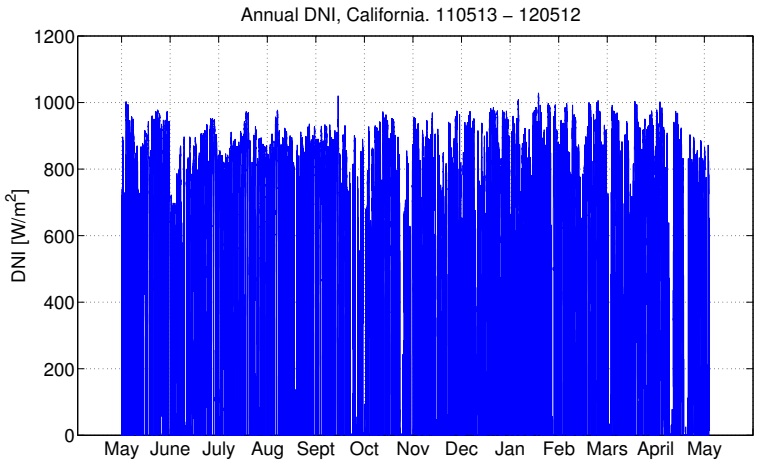

Figure 4.5: Direct Normal Irradiance (DNI) for Los Angeles, California 2011-05-13 to 2012-05-12

In order to see the long term differences between the two plants, DNI data accumulated over a year for the California site will be used for analysis. Note that the DNI data for a year in Figure 4.5 shows for daytime only, meaning that the data for nights when there is no insolation is removed.

4.2 Reference plant

In the reference plant a directly driven asynchronous machine is used as a generator. To initialize the system, the asynchronous machine is used as a starter. When the stirling engine gets up to working temperature the asynchronous machine is dragged by the stirling engine above synchronous speed which makes it act as a generator.

Since the directly driven asynchronous motor needs to be run in near constant speed, as described in Section 2.7.1, the same goes for the stirling engine because they are mechanically connected. This affect the overall efficiency since a stirling engine do not have the optimal operating point at a fixed speed for various power input, see Section 2.4.

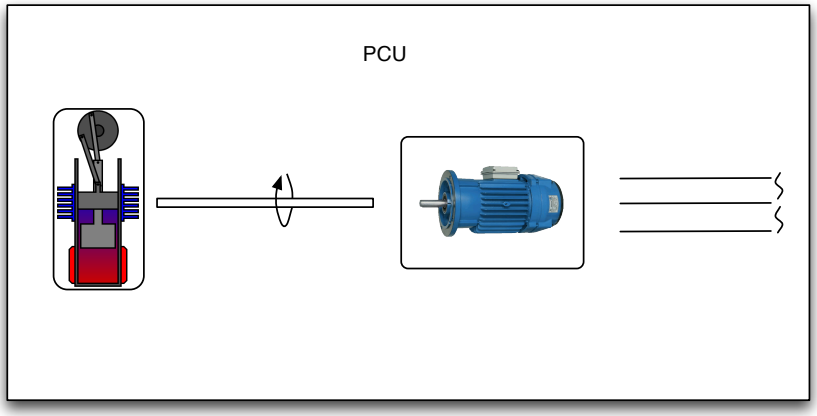

Figure 4.6: Reference PCU configuration.

The control principle is to try to keep the absorber temperature constant using a PI-controller in a inner loop and a P-controller in an outer loop. The controller changes the amount of working gas within the motor by opening valves to the high and low pressure tanks. The engine runs more efficient at higher pressures, but there is a maximum pressure allowed within the engine due to safety regulations and material properties. In this case, when locking the system to match the asynchronous speed of the generator, the system cannot handle a too high level of DNI input since the pressure will hit the maximum allowed limit at some point. When this occur, the system will have to ”detrack” the sun and will obviously not produce any power, since the heat from the sun is not focused onto the absorber.

This solution has the advantage that it uses very few parts and is durable, see Section 2.7.1. Since these kind of systems often are located at remote places, a minimum level of service is important. The most wear in the asynchronous motor is put on the bearings, which needs lubrication after two years based on 11 hours of use per day and 8000 hours between lubrications [25].

4.3 Concept plant

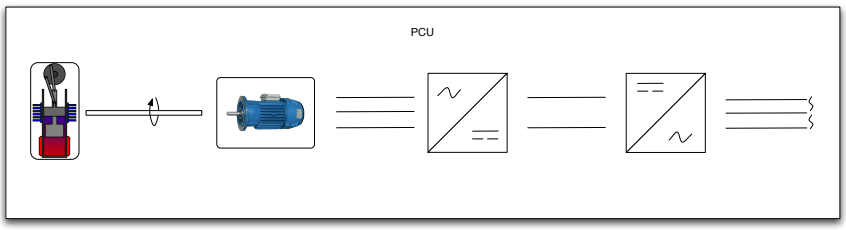

Figure 4.7: Concept PCU configuration.

In the concept plant an inverter controlled synchronous permanent-magnet (PM) drive is used as generator. This introduces the possibility of speed controlling the shaft of the generator and thus also the stirling engine since they are mechanically connected. The advantage of controlling the speed of the system is that it introduces the possibility of controlling the pressure in the system, and as mentioned in Section 2.4 the properties of the stirling engine says that the engine is more efficient at higher pressure. The absorber temperature will still be controlled as for the reference plant. The possibility of speed

controlling the drive shaft will be used for keeping the pressure in the engine close to the maximum allowed pressure within the engine. Controlling the pressure and drive shaft speed as described above means that the stirling engine will run at lowest possible speed while still maintaining a constant temperature of the absorber. Compared to the reference plant the concept plant will run at low speed when the DNI is low, this reduces the friction losses. At very high DNI when maybe the reference plant has to ”detrack” the sun, the speed of the PM shaft can be increased by alternating the frequency on the generator side of the power inverter and thus. A higher speed means that more heat is shuffled away from the heater into the stirling engine, and therefore cools the system enough to not needing to 'detrack' the sun.

4.4 Data gathering plan

In order to compare the two plants a mathematical model is derived, as presented in Section 3. The derived mathematical model is then to be implement in MATLAB Simulink using block schemas. In order to control the absorber temperature and the speed for the drive shaft two control systems are derived, as described in Section 3.3 and implemented in the model. Input to this system is the insolation and output will be how much power that could be supplied to the grid. Figure 3.5 shows simulation block diagram for the reference plant and Figure 3.7 shows simulation block diagram for the concept plant. To compare the two plants, solar irradiation over a year needs to be analysed. Because of the time scope transient behaviour within the motor can be neglected. Simulation of the suggested model is not possible to do over such a long time period due to that the required computation power is not available and it is not necessary either since the suggested model is dynamical and include transient behaviour. Therefore maps of all relevant variables is made by running the model at different levels of DNI at steady-state operating points, and then interpolated to make a map of the DNI spectra at which the plant can operate.

4.5 Load cycles

By looking at a different set of days as described in Section 4.1, different load characteristics is achieved. The modelled reference plant is tuned in to handle the solar insolation in California between 2011-05-13 to 2012-05-12, see Figure 4.5. It is an important step to measure maximum DNI levels for a site where a plant, of the reference plant type, is to be installed so that either the operating point for the stirling engine or the mirror area can be adjusted. For a real plant the mirror area is often adjusted to match stirling motor and generator specifications. But in this case a comparison between two plants is to be done. To do the comparison two plants with the same input is wanted, therefore the mirror area is kept the same for both plants. Instead the operating point of the stirling motor is optimized based on the location by changing the gear ratio between crank- and drive-shaft. Load characteristics for one of the sunniest days during the year is shown in Figure 4.8. A more cloudy and not as strong solar input the characteristics may look as in Figure 4.10. If the system would have been optimized in one location, but installed in for example Antalya in Turkey where the sun is more intense, the load characteristics is as presented in Figure 4.9. Here it is important to notice that the reference plant running in a fixed speed configuration stops producing power when the higher DNI would force the stirling engine to run with a higher pressure then allowed. If the CSP plant should be able to handle this higher DNI, the system have to be reconfigured with a new gearbox to increase the speed of the stirling engine.

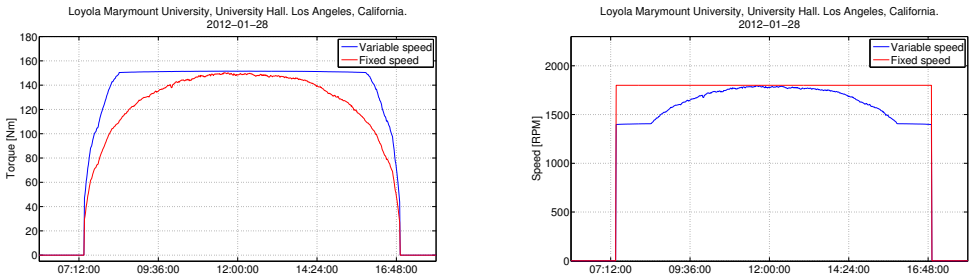

(a) Load Torque. (b) Load Speed.

Figure 4.8: Load characteristics for stirling engine based on an optimal level of DNI

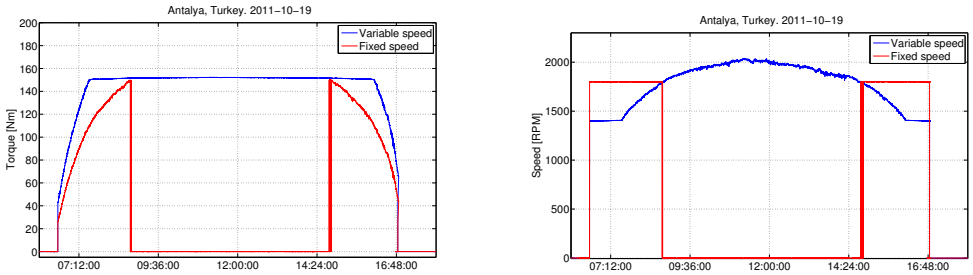

(a) Load Torque. (b) Load Speed.

Figure 4.9: Load characteristics for stirling engine based on a to high level of DNI

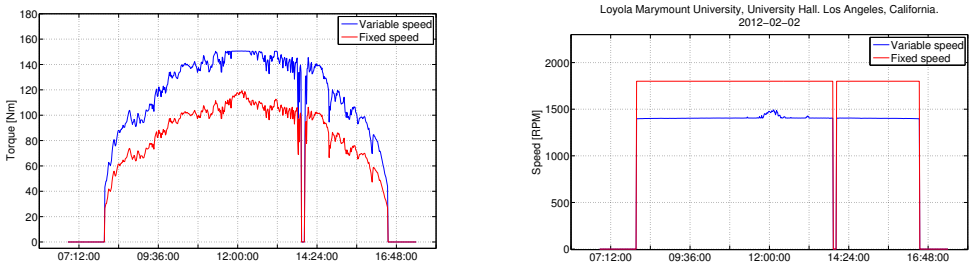

(a) Load Torque. (b) Load Speed.

Figure 4.10: Load characteristics for stirling engine based on a to low level of DNI

Chapter 5

Analysis

This chapter shows results from simulations made based on models of the reference and concept plant presented in Section 4. The reference plant is referred to as ”Fixed speed” in the figures and the concept plant is referred to as ”Variable speed”. First the performance of the two plants is presented. Based on the performance of the system, comparisons are made based on three reference days presented in Section 4.1. A comparison between the reference and concept plant over a year is then made. Finally, is a cost evaluation which aim to investigate the financial aspect of investing in a variable speed drive done.

5.1 Performance of the CSP-system

The simulated performance of the modelled system can be seen in Figure 5.1. Figure 5.1(a) shows that the stirling engine is up to 5% more efficient depending on the DNI and the total system efficiency can be improved by up to 3% at some DNI levels.

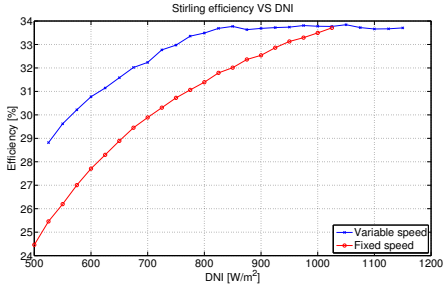

(a) Efficiency of stirling engine.

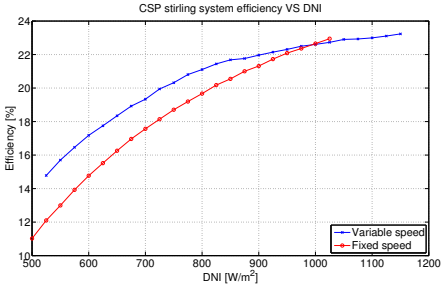

(b) Efficiency of CSP stirling power plant

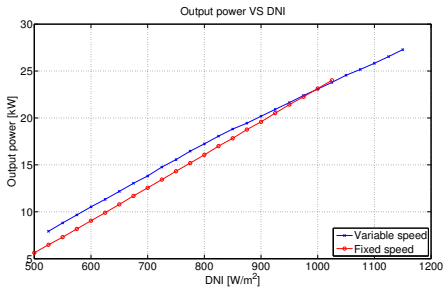

(c) Output power

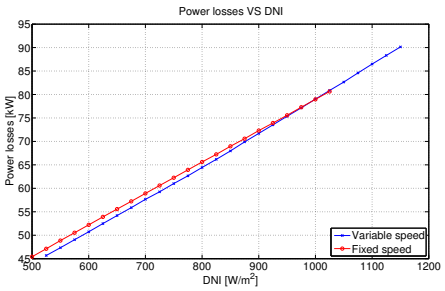

(d) Losses in CSP stirling power plant

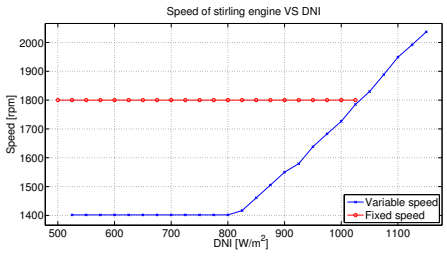

(e) Speed of stirling engine vs DNI

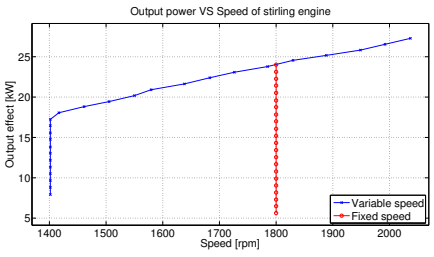

(f) Output power vs Speed of stirling

Figure 5.1: Performance of the system.

5.2 Output from the CSP-system

Three days with different insolation characteristics is presented in this chapter, a cloudy day, a day optimized for the reference plant and a day with too much insolation for the reference plant. This three days aim to describe the three type of characteristics that is expected during a day. Except for those days when almost no solar radiation reaches the plants, but then the output would be zero for both plants and thus no comparison is needed.

5.2.1 Non-optimized day

If the daily insolation exceeds the level that the reference plant is optimized for, see Figure 4.4, the system have to stop producing power, as described in Section 4.5. If a day like this occurs at the location where the plant is installed it gives a very low total amount of produced power, see Figure 5.2, due to the forced inactivity. This shows the importance of preparation work where measurements is made so that the reference plant operating point can be altered to match the maximum insolation received.

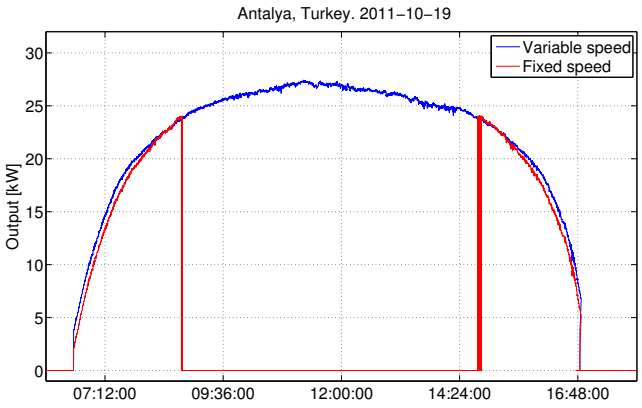

Figure 5.2: Output from the two plants for a non-optimized insolation level.

5.2.2 Optimized day

When looking at an optimal day, see Figure 4.2, where the level of the insolation reaches the level that the reference plant is optimized for. The difference in output between the two systems is quite small, see Figure 5.3. The reason why the output for the reference plant is higher than for the concept plant at the maximum DNI for the day is because that the efficiency for the generator solution is higher in the reference plant.

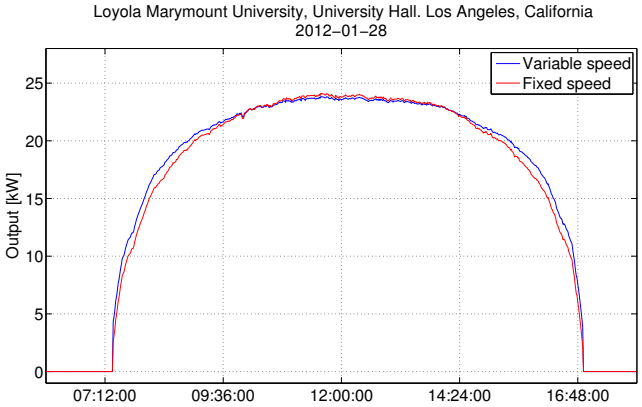

Figure 5.3: Output from the CSP model for an optimized insolation level.

5.2.3 Cloudy day

During a cloudy day, see Figure 4.3, where parts of the sun insolation is blocked in the atmosphere, the daily output for the reference and concept plant is presented in Figure 5.4. The difference in output between the two plants is quite large since friction losses are much higher in the reference plant then for the concept plant.

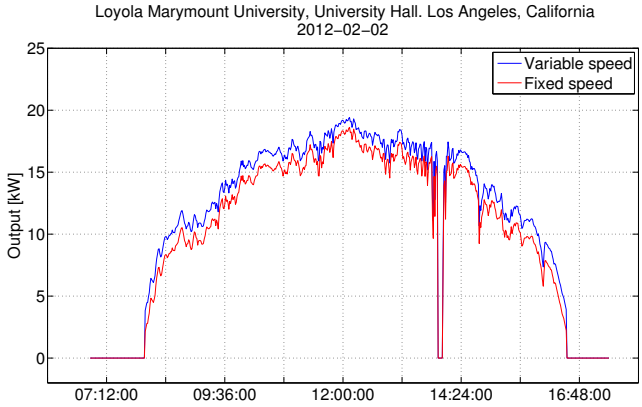

Figure 5.4: Output from the CSP model for a cloudy day.

5.2.4 Annual output

The output from May 2011 to May 2012 can be seen in Figure 5.5. Since the reference plant in this thesis is optimized for the sunniest day during the year, the scenario described in Section 5.2.1 never occurs, however it is an interesting result for discussion purposes.

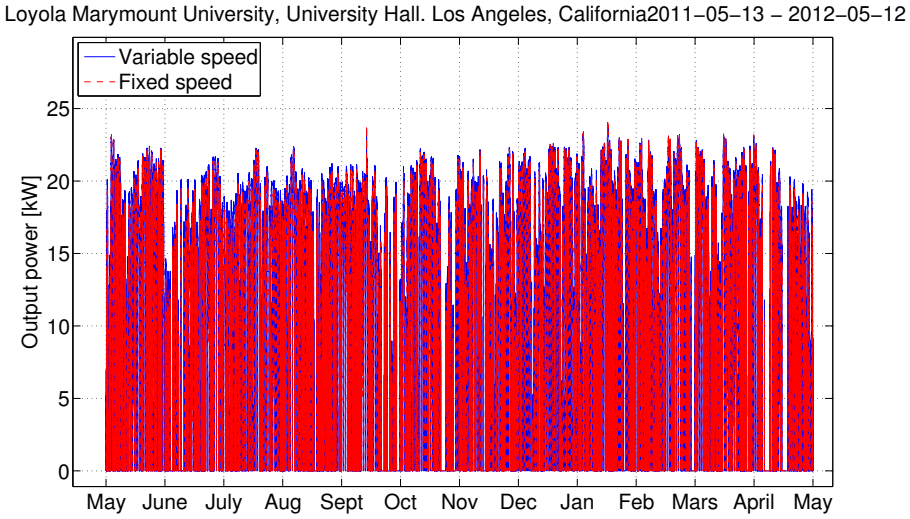

Figure 5.5: Output from the two plants over a year.

5.2.5 Comparison of outputs

By integrating the area below the output curves with respect to time, the output is expressed in terms of kWh. The improvement of output using the variable speed system instead of the fixed speed system is calculated as

$$\frac{kWh_{Variable\,speed} - kWh_{Fixed\,speed}}{kWh_{Fixed\,speed}} \tag{5.1}$$

and the result can be seen in Table 5.1. The annual extra output of 6.68% can be seen as an extra profit shared equal between the CSP producer and the power plant investor. This gives approximately 3.3% extra sales margin on the product.

Case	Fixed speed [kWh]	Variable speed [kWh]	Improvement [%]
Non-optimized day	73.2	232.5	217.6
Optimized day	189.7	193.4	1.95
Cloudy day	109.5	120.2	9.77
Annual	37968	40506	6.68

Table 5.1: Output comparison between the two systems

5.3 Cost evaluation

By assuming that the electricity price is equal to the average price in USA, 0.10 USD [26] , the extra power produced by the system gives an extra income of 254 USD per year. It is assumed that a CSP system should be functional for at least 25 years.

$$PV = \sum_{i=1}^{25} \frac{254_i}{(1+0.05)^i} \approx 3600 \tag{5.2}$$

Using this in the net present value-method, see Section 2.9, with an interest of 5% and with no residual value is seen in (5.2).

However, by changing to a new technology, new costs is added to the project. An air-cooled PMSG is about the same size and weight as an asynchronous generator and costs about the same as well [27], approximately 1500 USD. Additional cost for the power converter system (as described in Section 2.8) is also added. It is assumed the cost of the power converter is about the half of the cost of the PMSG. Costs for implementing this solution is hard to estimate, since it is spread out over the number of sold products, and therefore it is put as a variable in costs calculations. Wear in the system due to the new speed operating range is not evaluated, the most uncertain part is how the stirling engine can handle running on more or less maximum pressure all the time. Other maintenance costs required for the reference plant compared to the concept plant is not evaluated either and therefore the maintenance cost is put as a variable in cost calculations. Based on this information the net present value per unit is calculated as

$$G = I_{PMSG} + I_{converter} + I_{maintenance} + \frac{I_{implementation}}{n_{sold\,units}} - I_{AS} \tag{5.3}$$

$$NPV = 2850 - I_{maintenance} - \frac{I_{implementation}}{n_{sold\,units}} \tag{5.4}$$

Important to consider is that the CSP system is to be sold in bigger parks giving many MW output. For a small 2MW power plant site, 67 dish stirling plants, the net present value without considering maintenance and implementation costs is about 191 000 USD.

Chapter 6

Conclusions

6.1 Results from present work

The differences between fixed speed plant using a cheaper directly driven asynchronous generator compared to the variable speed case with a conversion system depends on the installation site. Depending on the insolation characteristics of the location the improvement using a more expensive variable speed solution is more or less suitable from a financial point of view. On the site used for the analysis in this thesis, the improvement is around 6.68% over a year with variations between 1.95% for an optimized day and 9.77% for a day with more clouds. The big profit of the variable speed system is mainly during the times of the day when the DNI is lower, during the time with highest DNI possible that the system is optimized for, the fixed speed system is actually a bit more efficient. Lower DNI implies that the stirling engine can be run slower and increasing its efficiency up to approximately 5%.

Based on the results from the cost evaluation the extra energy produced is considered to be enough if the production of the dish stirling plants is done in series production. However, to be able to make a more precise conclusion whether it is economical feasible or not, some additional analysis need to be made. The impact on the system when having a speed controller needs to be evaluated. An estimation of implementation costs tied to the investment of this system need to be done.

An important aspect of the results is the importance of optimizing the system, especially in the reference case. If the reference system is not optimized for the installation site, it might not ever be at the top of the efficiency curve, or it might be under-dimensioned and not producing power during the most solar intensive days. By introducing the variable speed approach, the system is more independent of variations of solar input and will always be at it's top efficiency for the current DNI. Also, the system can handle the extreme cases with very high DNI.

6.2 Future work

This thesis presents a model of a stirling CSP system. The derived model is based on many assumptions due to lack of measured variables on e.g the regenerator, the heater etc. The next step for having a better model is to measure the efficiency of the subsystems and temperatures within each systems to introduce good validation data. The model derived in this thesis has been adjusted to match a real stirling CSP system, however the introduced losses might not be placed correct in the system.

Another interesting point is to evaluate the difference in output from the two cases presented with solar input from other geographical sites. It is interesting to see how the results from the comparison is affected when considering geographical sites where the insolation vary more over a year. Added to

this, it is also interesting to see how many solar days is needed during a year to make the investment in a stirling CSP plant profitable.

Next thing is to get hands on and firstly find durable products for this implementation, and secondly make a sharp implementation of the proposed variable speed system. Also, further analysis of the impact of the cooling system needs to be done. In the derived model, a constant cooling of the system is used unrelated to the actually need. When the system runs at lower DNI, it probably wont need the same cooling effect as when running at highest possible DNI. It was attempted to find information on pricing for small-sized lightweight water cooled PM machines, but due to the fact that this is a area with much development going on right now it was hard to find any solid information. This is mainly driven by the development of electrical or hybrid cars and is something that might be easier to find information about in coming years.

Appendix A

Control of frequency converter

A.1 Space Vector Modulation (SVM)

SVM is used for determining the duty cycles that are used by a PWM controller to generate sine waves for AC. The method has been very popular because of its simplicity [28]. It provides an accurate control of the voltage amplitude and voltage frequency. It is based on a space vector representation of the AC voltage. Based on the switch set-up in the converter, see Section 2.8.1, there is a total of 8 different state voltages possible each represented by a vector. 6 active states where the output voltage is non-zero and 2 states where the output voltage is zero.

SVM uses the stationary $\alpha\beta$ reference frame to represent the vectors. Where the reference voltage space vector U^* is calculated as:

$$\overline{U}^* = u_\alpha + ju_\beta = \frac{2}{3}(u_{aref} + e^{j\frac{2\pi}{3}}u_{bref} + e^{-j\frac{2\pi}{3}}u_{cref}) \tag{A.1}$$

The active vectors divide the plane in to 6 different sectors where U^* is calculated from the two adjacent vectors, which vectors that is the two adjacent vectors depends on the U^* phase angle α. In Figure A.1 the reference vector U^* is in sector 1 and are thus defined by state voltage vectors $\overline{U}_1$ and $\overline{U}_2$. $\overline{U}_1$ is the voltage represented by the vector $(1, 0, 0)$ which corresponds to switch S_a in Figure 2.10 is conducting and the inverted switches S'_b and S'_c are conducting.

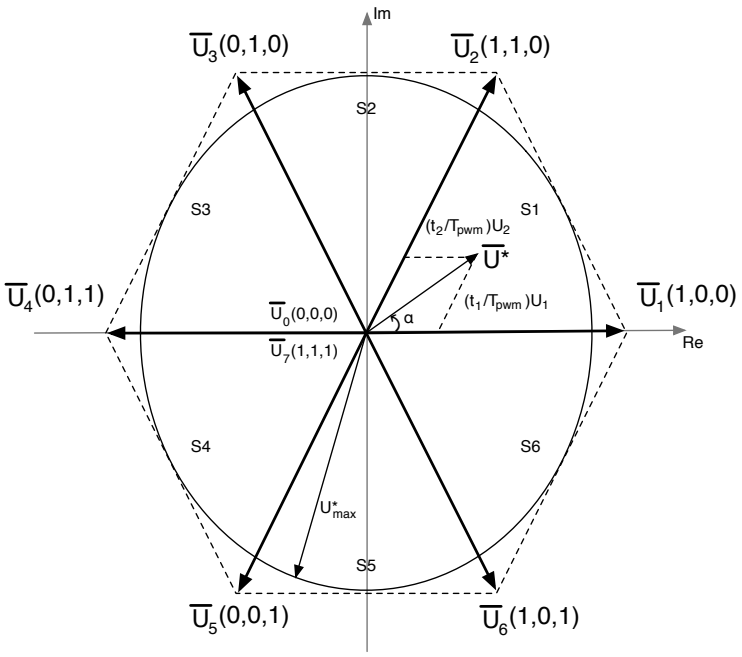

Figure A.1: Space vector representation for a 3 phase converter

The maximum length that U^* can adopt is $U^*_{max} = U_{dc}/\sqrt{3}$. To reduce the number of switching commutations, the switching in Figure A.1 occur in following order: (0,0,0), (1,0,0), (1,1,0), (1,1,1). Representation of voltage vectors in SVM applies that the zero states are symmetrical:

$$t_7 = t_0 = \frac{T_{pwm} - t_1 - t_2}{2} \tag{A.2}$$

where t_0, t_1, t_2, t_7 are time durations of the applied vectors and T_{pwm} represent the grid switching frequency. Calculation of U^* in Figure A.1 is done as:

$$\overline{U}^* = \overline{U}(1,0,0)\frac{t_1}{T_{pwm}} + \overline{U}(1,1,0)\frac{t_2}{T_{pwm}} \tag{A.3}$$

where

$$\overline{U}(1,0,0) = \frac{2}{3}U_{dc} \tag{A.4}$$

$$\overline{U}(1,1,0) = \frac{2}{3}U_{dc}(\frac{1}{2} + j\frac{\sqrt{3}}{2} \tag{A.5}$$

From Figure A.1 it can be seen that

$$\overline{U}^* = U^*(\cos\alpha + j\sin\alpha) \tag{A.6}$$

holds.

Using (A.3), (A.6) and dividing the imaginary and real parts equations for time duration t_1 and t_2:

$$t_1 = \sqrt{3}\frac{U^*}{U_{dc}} T_{pwm} \sin(\frac{\pi}{3} - \alpha) \tag{A.7}$$

$$t_2 = \sqrt{3}\frac{U^*}{U_{dc}} T_{pwm} \sin(\alpha) \tag{A.8}$$

When t_1 and t_2 have been calculated the remaining sample time is reserved for the zero voltage vectors U_0 and U_7. Calculation of duty cycles for sector 1:

$$D_a = \frac{t_1 + t_2 + t_0/2}{T_{pwm}} \tag{A.9}$$

$$D_b = \frac{t_2 + t_0/2}{T_{pwm}} \tag{A.10}$$

$$D_a = \frac{t_0/2}{T_{pwm}} \tag{A.11}$$

A.2 Field Oriented Control

Control of the Permanent Magnet Synchronous Generator (PMSG) can be done using a variety of different control strategy's. A commonly used strategy is the Field Oriented Control (FOC) principle which uses the rotor position and rotor speed to control the torque of the PMSG indirectly [29] in a closed-loop control structure. This is done by controlling the stator currents of the PMSG. The control strategy is expressed in the rotor reference frame dq. This greatly simplifies calculations because this makes the system time invariant, as a result of this the machine parameters are constant. Expressing the torque in the dq reference frame:

$$T_e = \frac{3}{2}\frac{p}{2}\Psi_m i_{sq} \tag{A.12}$$

shows that the torque can be controlled by controlling the current q if the permanent flux linkage, Ψ_{sq}, is constant. To control the stator currents the torque angle is controlled. There are several strategy's for controlling the torque, three commonly used are [30]:

- Constant angle control - The torque angle, α, is controlled to be kept at $90\,^{\circ}\mathrm{C}$. The d-axis current is controlled to be 0. This makes control straightforward since then, according to (A.12), the torque can be controlled by controlling the q-axis current.
- Unity power factor - The active power and the apparent power is controlled to be equal.
- Constant stator flux - The stator flux amplitude vector is kept equal to the permanent magnet flux vector, which also means that it is kept constant since the permanent magnet flux vector is considered to be constant.

Constant angle control is chosen as control principle because of it's simplicity.

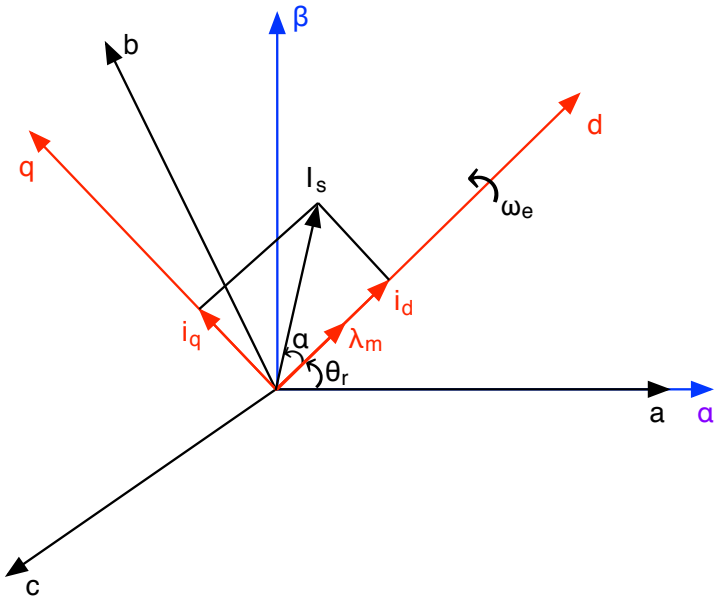

Figure A.2: Field Oriented Control vector diagram

In Figure A.2 α is the torque angle, θ is the load angle and I_s is the stator current vector. The stator current consists of the two components i_{sd} and i_{sq}:

$$I_s = i_{sd} + ji_{sq} \tag{A.13}$$

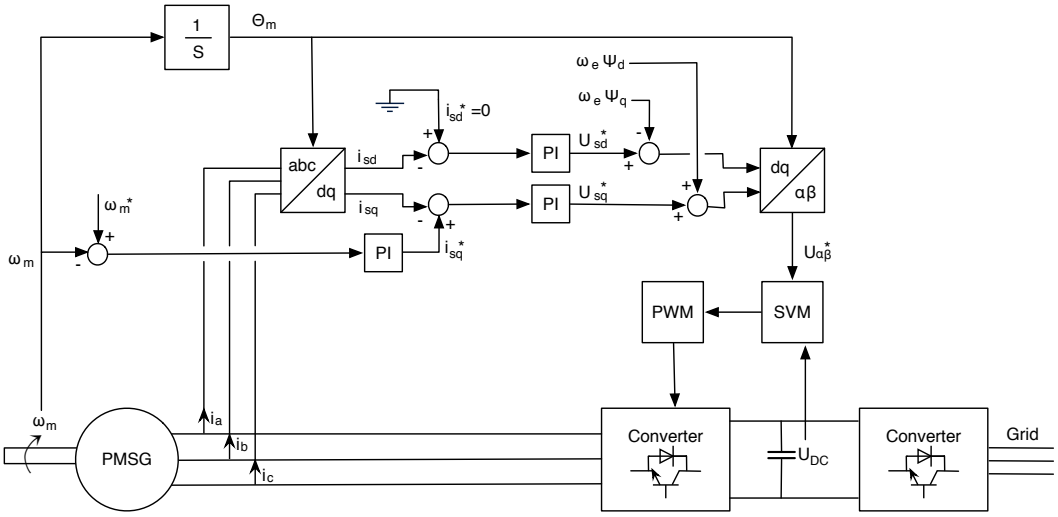

Figure A.3: Proposed control system using Field Oriented Control.

In Figure A.3 the proposed control system using FOC is presented. ω_m is the mechanical speed in

rev/min and ω_e is the electrical speed in rad/s. For the q-axis there is an outer loop where the speed is controlled. The signal from that controller is then fed to the current controller of the q-axis. The d-axis current reference is constant set to 0 since constant angle control is used. To generate the voltages $u_{sq,sd}$ a decoupling factor derived from the stator voltage equations in the dq-frame is used.

$$u_{sq} = R_s i_{sq} + \frac{d\Psi_q}{dt} + \omega_e \Psi_d \tag{A.14}$$

$$u_{sd} = R_s i_{sd} + \frac{d\Psi_d}{dt} + \omega_e \Psi_q \tag{A.15}$$

Both (A.14) and (A.15) has the back-emf as common term. By subtracting the back-emf from the two equations they are made independent of each other. The control system proposed in Figure A.2 uses sensors to measure the mechanical speed and position of the machine shaft, there are also other techniques available that uses sensor-less control which estimates speed and position from the phase currents of the machine [31]. Coordinate transformations between the abc, $\alpha\beta$ and dq reference is not explained in this thesis, see [32].

Appendix B

Overview of Simulink models

In this appendix, overview of the simulink models derived in this thesis is presented. The intention of this is to show how the modelling problem was attacked and how the thoughts of the system in the authors minds have been.

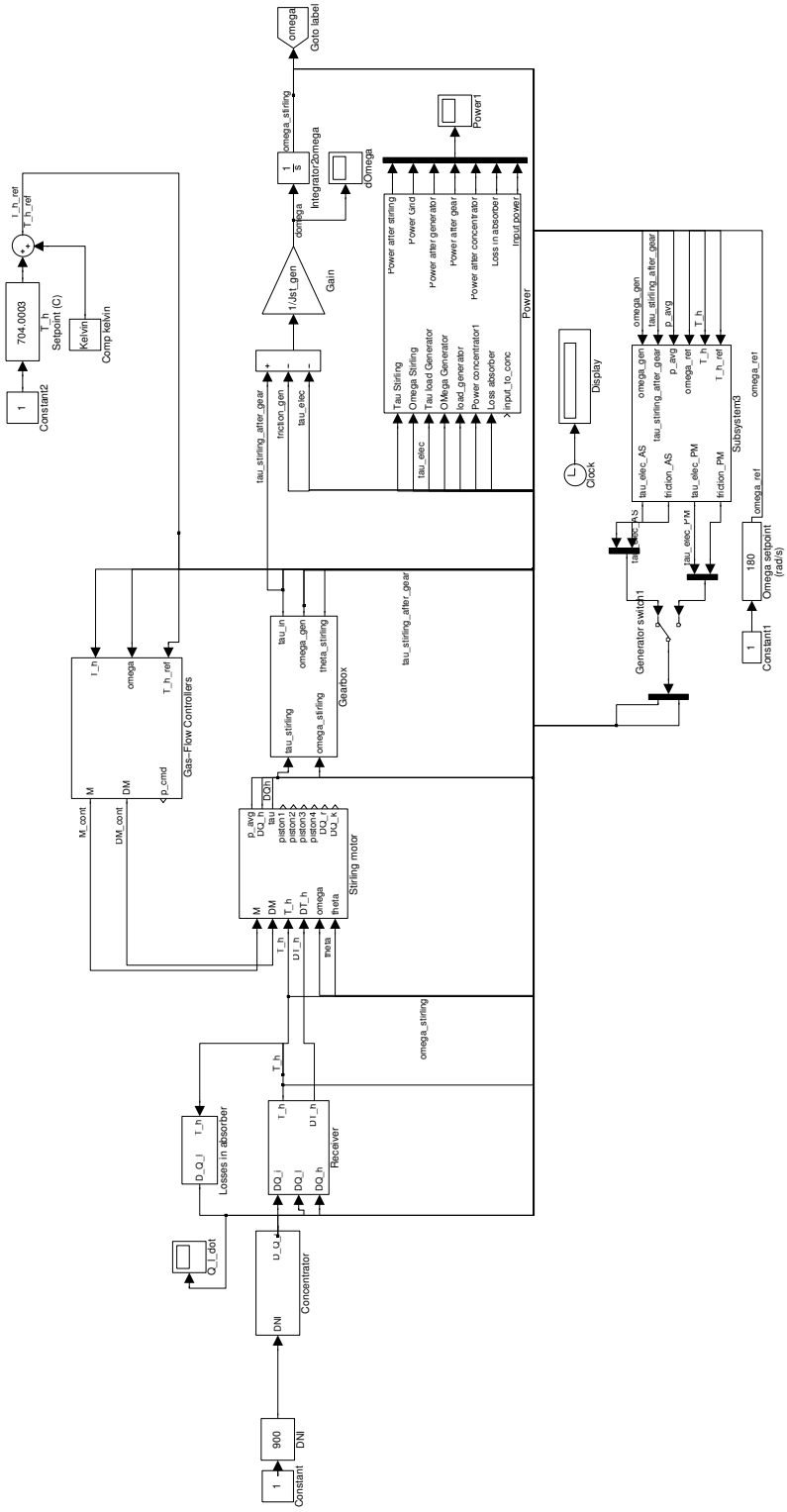

Figure B.1: Main model.

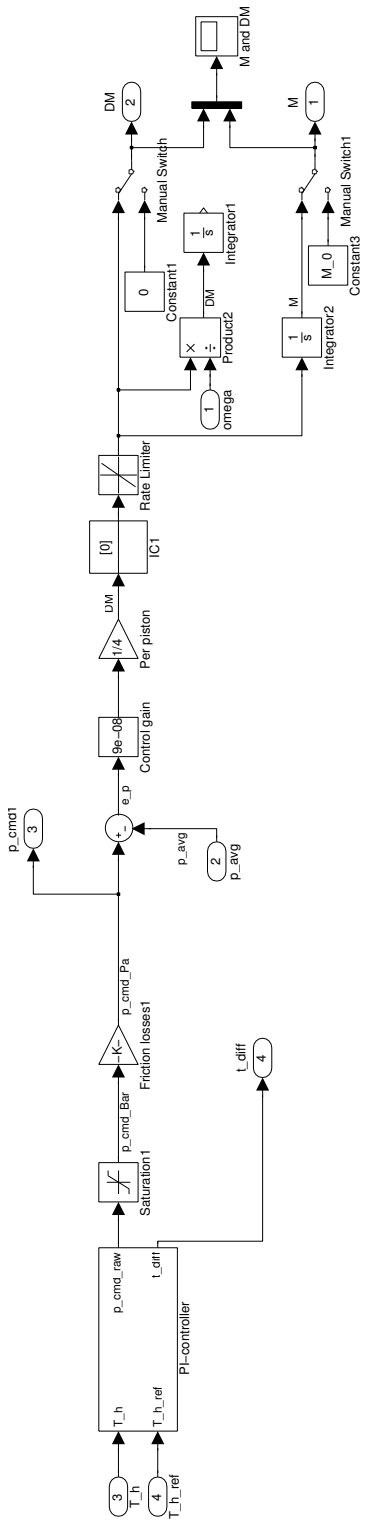

Figure B.2: Control system layout

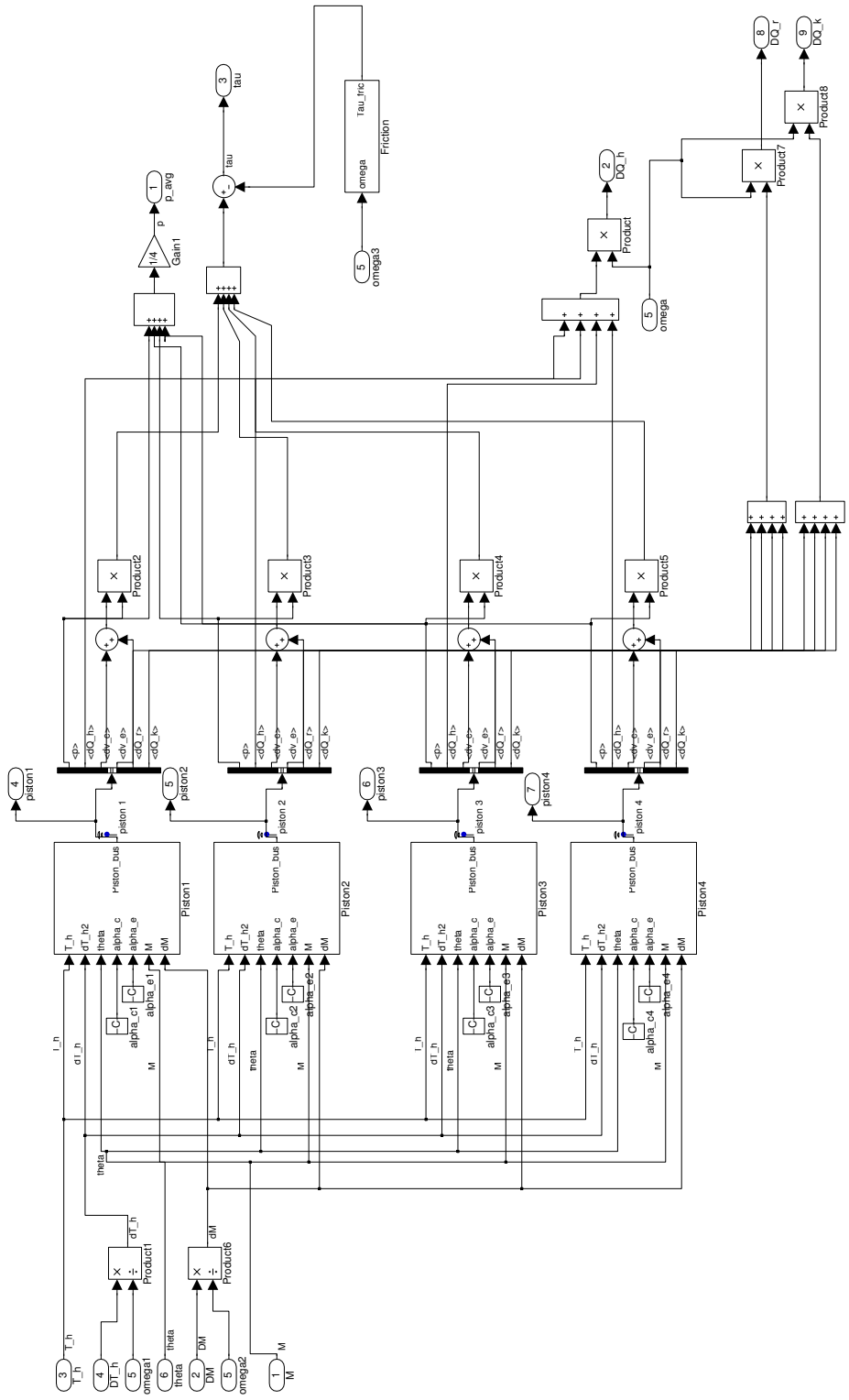

Figure B.3: Model of the stirling engine.

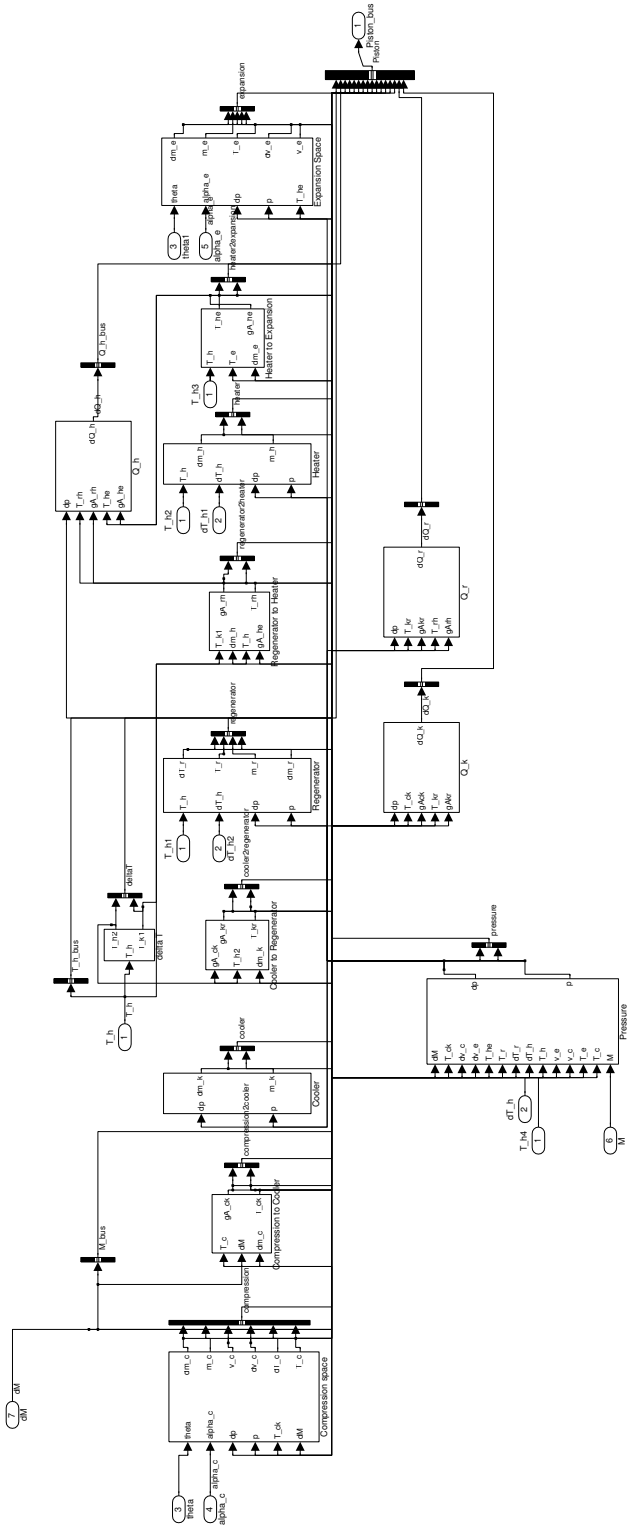

Figure B.4: One of the four engine compartments

References

[1] National Renewable Energy Labatory (NREL), "Solar and Wind Energy Resource Assessment (SWERA)," ONLINE, 2012-05-21, http://maps.nrel.gov/swera.

[2] M. A. Green, K. Emery, Y. Hishikawa, and W. Warta, "Solar cell efficiency tables (version 37)," 2010, http://onlinelibrary.wiley.com/doi/10.1002/pip.1088/pdf.

[3] M. R. Patel, *Wind and solar power systems*. CRC Press. Boca Raton London New York Washington, D.C.. 0-8493-1605-7, 1999.

[4] B. Washom, "Parabolic dish stirling module development and test results," in *Paper No. 849516, Proceedings of the IECEC, San Francisco, CA*, 1984.

[5] National Renewable Energy Labatory (NREL), "Power tower projects," ONLINE, 2012-03-07, http://www.nrel.gov/csp/solarpaces/power_tower.cfm.

[6] U.S. Energy Information Administration, "Early Annual Energy Outlook 2010 with Projections to 2035," ONLINE, 2012-03-07, www.eia.doe.gov/oiaf/aeo/.

[7] J. L. Sawin and E. Martinot, "Renewables bounced back in 2010, finds ren21 global report," *Renewable Energy World*, September 2011.

[8] European Renewable Energy Council (EREC), ONLINE, 2012-03-07, www.erec.org.

[9] O. Langniβ, J. Diekmann, and U. Lehr, "Advanced mechanisms for the promotion of renewable energy - models for the future evolution of the german renewable energy act," *Energy Policy 37*, pp. 1289–1297, 2009, journal homepage: www.elsevier.com/locate/enpol.

[10] E. Kirschbaum, "Germany sets new solar power record, institute says," ONLINE, BERLIN, May 26, 2012, http://www.reuters.com/article/2012/05/26/us-climate-germany-solar-idUSBRE84P0FI20120526.

[11] W. B. Stine and R. B. Diver, "A compendium of solar dish/stirling technology," Mechanical Engineer at California State Polytechnic University and Solar Thermal Technology Department at Sandia National Laboratories, Compendium, 1994.

[12] W. Martini, "Stirling engine design manual, second edition," Jan 1983, available: http://www.scribd.com/doc/20191898/Stirling-Engine-Design-Manual.

[13] G. T. Reader and C. Hooper, *Stirling Engines*. E. & F.N. Spon, 1983, ISBN #0419124004.

[14] A. Hughes, *Electric Motors and Drives*, 3rd ed. Newnes, 2006, ISBN-13: 978-0-7506-4718-2.

[15] M. J. Ryan and R. D. Lorenz, "A "Power-Mapping" Variable-Speed Control Technique for a Constant-Frequency Conversion System powered by a IC Engine and PM Generator," *Industry Applications Conference, 2000. Conference Record of the 2000 IEEE*, vol. 4, pp. 2376–2382, oct, 2000, ISBN: 0-7803-6401-5.

[16] H. Li and Z. Chen, "Optimal direct-drive permanent magnet wind generator systems for different rated wind speeds," *Power Electronics and Applications, 2007 European Conference on*, 2-5 Sept 2007, conference Publication.

[17] H. Polinder, F. F. A. van der Pijl, G.-J. de Vilder, and P. J. Tavner, "Comparison of direct-drive and geared generator concepts for wind turbines," *IEEE Transactions On Energy Conersion*, vol. 21, no. 3, pp. 725–733, Sept 2006, digital Object Identifier 10.1109/TEC.2006.875476.

[18] D. F. Howard, "Modeling, simulation, and analysis of grid connected dish-stirling solar power plants," Master's thesis, Georgia Institute of Technology, August 2010.

[19] Ohio University, Russ College of Engineering and Technology, Mechanical Engineering Department, "Regenerator Simple Analysis," ONLINE, 2012-03-22, http://www.ohio.edu/mechanical/stirling/simple/regen_simple.html.

[20] T. Finkelstein, "Thermodynamic Analysis of Stirling Engines," *J. Spacecraft Rockets*, vol. 4, pp. 1184–1189, 1967.

[21] SIEMENS, "Test certificate of induction motor," type: 16BG 207-4AA60-Z, Serial no: 13800601. Test no: 24415-A.

[22] A. Rabiei, T. Thiringer, and J. Lindberg, "Application of Non-linear Programming in Loss Minimization Current Vector Control of PMSM Including the Core Losees," *International Conference on Electrical Machines 2012, ICEM'12, Marseille*, September 2012.

[23] R. Stanton, C. Ayers, L. Marlino, J. Chiasson, and T. Burress, "Evaluation of 2004 Toyota Prius Hybrid Electric Drive System," May 2006, Oak Ridge National Laboratory. Report no: ORNL/TM-2006/423.

[24] National Renewable Energy Labatory (NREL), "Solar Resource & Meteorological Assessment Project (SOLRMAP) Loyola Marymount University, University Hall, Los Angeles, California," ONLINE, 2012-05-21, http://www.nrel.gov/midc/lmu/.

[25] *Electric Motors*, Lönne, Kastellgatan 5, S-254 66, Helsingborg, 2009.

[26] U.S Energy Information Administration, "Eletricity data browser," ONLINE, 2012-05-21, http://www.eia.gov.

[27] M. T. Ameli, S. Moslehpour, and A. Mirzaie, "Feasibility study for replacing asynchronous generators with synchronous generators in wind farm power stations," in *Proceedings of The 2008 IAJC-IJME International Conference*, 2008, ISBN: 978-1-60643-379-9.

[28] M. Kawmierkowski and R. Krishnan, "Control in power electronics. selected problems," *Academic Press*, 2002, ISBN 0-12-402772-5.

[29] M. O. Mora, "Sensorless vector control of pmsg for wind turbine applications," Master's thesis, Aalborg University, 2009.

[30] Z. Xiaotan, L. Chongjian, L. Yaohua, and W. Chengsheng, "Analysis of a large power pmsm using different control methods," vol. 1, Institute of Electrical Engineering Chinese Academy of Science, Beijing and Automation Research and Design Institute of Metallurgical Industry, Beijing. Proceedings of the Eighth International Conference on Electrical Machines and Systems, September 2005, pp. 416–421.

[31] J. Zambada, *Sensorless Field Oriented Control of PMSM Motors*, 2007.

[32] I. Jadric, "Modeling and control of a synchronous generator with electronic load," Master's thesis, Virginia Polytechnic Institute and State University, January 1998.